

AWARD NUMBER: W81XWH-19-1-0166

TITLE: miRNA-Mediated Rescue of NK Cell Cytotoxicity Against Drug-Resistant Quiescent Leukemia Stem Cells

PRINCIPAL INVESTIGATOR: Perrotti, Danilo M.D., Ph.D.

CONTRACTING ORGANIZATION: University of Maryland, Baltimore, MD

REPORT DATE: October 2022

TYPE OF REPORT: Final

**PREPARED FOR: U.S. Army Medical Research and Development Command
Fort Detrick, Maryland 21702-5012**

DISTRIBUTION STATEMENT: Approved for Public Release; Distribution Unlimited

The views, opinions and/or findings contained in this report are those of the author(s) and should not be construed as an official Department of the Army position, policy or decision unless so designated by other documentation.

REPORT DOCUMENTATION PAGE			<i>Form Approved</i> <i>OMB No. 0704-0188</i>		
Public reporting burden for this collection of information is estimated to average 1 hour per response, including the time for reviewing instructions, searching existing data sources, gathering and maintaining the data needed, and completing and reviewing this collection of information. Send comments regarding this burden estimate or any other aspect of this collection of information, including suggestions for reducing this burden to Department of Defense, Washington Headquarters Services, Directorate for Information Operations and Reports (0704-0188), 1215 Jefferson Davis Highway, Suite 1204, Arlington, VA 22202-4302. Respondents should be aware that notwithstanding any other provision of law, no person shall be subject to any penalty for failing to comply with a collection of information if it does not display a currently valid OMB control number. PLEASE DO NOT RETURN YOUR FORM TO THE ABOVE ADDRESS.					
1. REPORT DATE October 2022		2. REPORT TYPE Final		3. DATES COVERED 01Jul2019-30Jun2022	
4. TITLE AND SUBTITLE miRNA-Mediated Rescue of NK Cell Cytotoxicity Against Drug-Resistant Quiescent Leukemia Stem Cells			5a. CONTRACT NUMBER W81XWH-19-1-0166		
			5b. GRANT NUMBER		
			5c. PROGRAM ELEMENT NUMBER		
6. AUTHOR(S) Perrotti, Danilo M.D., Ph.D. (Principal Investigator) Trotta, Rossana Ph.D (Co-Principal Investigator) E-Mail: dnerrotti@som.umaryland.edu			5d. PROJECT NUMBER		
			5e. TASK NUMBER		
			5f. WORK UNIT NUMBER		
7. PERFORMING ORGANIZATION NAME(S) AND ADDRESS(ES) University of Maryland Baltimore 620 W. Lexington Street, 4 th Floor Baltimore, MD 21201			8. PERFORMING ORGANIZATION REPORT		
9. SPONSORING / MONITORING AGENCY NAME(S) AND ADDRESS(ES) U.S. Army Medical Research and Development Command Fort Detrick, Maryland 21702-5012			10. SPONSOR/MONITOR'S ACRONYM(S)		
			11. SPONSOR/MONITOR'S REPORT NUMBER(S)		
12. DISTRIBUTION / AVAILABILITY STATEMENT Approved for Public Release; Distribution Unlimited					
13. SUPPLEMENTARY NOTES					
14. ABSTRACT Qualitative and quantitative defects in natural killer (NK) cells is a feature contribute to survival of BCR-ABL1 tyrosine kinase inhibitor (TKI)-resistant quiescent leukemia-initiating stem cells (qLSCs) in TKI-treated chronic myelogenous leukemia (CML) patients. The goal of this project was to determine whether miR-155 expression confers to NK cells the ability to overcome the BM mesenchymal stem cell (MSC) and hypoxia-induced inhibitory effects on their proliferation and anti-cancer cytotoxicity, and efficiently kill TKI-resistant CML qLSCs. We found that expression of pre-miR-155 but not mature miR-155 markedly and significantly increased absolute numbers of BM NK cells and their cytotoxic activity against leukemic but not normal quiescent (CFSE ^{max}) LSCs. Moreover, we found that BM-induced NK cell inhibition was dependent on increased miR-300. Mechanistically we found that pre-miR-155 activity was dependent on increased SET and SHIP1 inhibition, and on FAS and DR5 expression, which would make CML qLSCs more susceptible to NK cell killing.					
15. SUBJECT TERMS None listed.					
16. SECURITY CLASSIFICATION OF:			17. LIMITATION OF ABSTRACT	18. NUMBER OF PAGES	19a. NAME OF RESPONSIBLE PERSON
a. REPORT Unclassified	b. ABSTRACT Unclassified	c. THIS PAGE Unclassified			Unclassified
					19b. TELEPHONE NUMBER <i>(include area code)</i>

TABLE OF CONTENTS

	<u>Page</u>
1. Introduction	4
2. Keywords	4
3. Accomplishments	4
4. Impact	11-12
5. Changes/Problems	12-13
6. Products	14-15
7. Participants & Other Collaborating Organizations	16-17
8. Special Reporting Requirements	17
9. Appendices	18-45

1. INTRODUCTION:

Qualitative and quantitative defects in natural killer (NK) cells is a feature contribute to survival of BCR-ABL1 tyrosine kinase inhibitor (TKI)-resistant quiescent leukemia-initiating stem cells (qLSCs) in TKI-treated chronic myelogenous leukemia (CML) patients. Our preliminary data indicate that the decrease in NK cell numbers and their inability to kill CML qLSC may result from unbalanced levels of the bone marrow microenvironment (BMM)-regulated miR-155 and miR-300 in NK cells. Thus, we proposed to determine whether altering the miR-155/miR-300 ratio by increasing miR-155 expression confers to NK cells the ability to overcome the BM mesenchymal stem cell (MSC) and hypoxia-induced inhibitory effects on their proliferation and anti-cancer cytotoxicity, and efficiently kill TKI-resistant CML qLSCs *in vitro* and *in vivo*. This study might serve as proof-of-concept for developing miRNA-based NK cell immunotherapies for the several stem cell-derived malignancies with dysfunctional NK cells.

2. KEYWORDS:

Leukemia, CML, BCR-ABL1, NK cells, miRNAs, miR-155, miR-300, quiescent LSC, MSC, hypoxia, immunotherapy.

3. ACCOMPLISHMENTS:

What were the major goals of the project?

The major goals of this funded project were:

Aim#1 To assess whether sustained miR-155 expression rescues NK cell killing of TKI-resistant qLSCs by determining whether 1A) constitutive miR-155 expression enhances NK cell killing of quiescent CML LSCs and restores selective cytotoxicity against leukemic but not normal HSCs in primary NK cells from leukemic animals *in vitro*; and 1B) constitutive miR-155 expression alone or associated with miR-300 downregulation override the hypoxia- and MSC-induced NK cells growth arrest and impaired cytotoxicity toward patient-derived qLSCs.

Aim#2 To determine the *in vivo* therapeutic potential of miR-155-activated NK cell anti-LSC cytotoxic activity by 2A) generation and *in vitro* functional characterization of BMM-resistant NK-92-155/anti-300 cells.; and 2B) assessing NK-92-155/300 cytotoxicity against CML qLSCs in CML mouse PDXs.

What was accomplished under these goals?

This is the final technical outcome of the experiments performed from 7/1/2019 (from 8/30/2019 – date of ACURO approval) until 6/30/2022. Note that all experimental activities have been suspended on March 18th, 2020 and restarted at normal pace in Fall 2021 due to COVID-19.

Project goals remained the same. We successfully completed all experimental tasks proposed in Aims 1A, 1B and 2A. Unfortunately, results indicated that the effect of miR-155 mimic RNA oligonucleotides in human NK cells were not as strong as in mouse NK cells and did not sufficiently counteract the inhibitory effects exerted by bone marrow (BM) microenvironment (BMM) factors (e.g., MSCs and hypoxia). This and COVID-19 pandemic strongly precluded feasibility of experiments proposed in SOW Task 2B. As an alternative, we followed the Reviewers' panel suggestions and investigated the miR-155- and miR-300-dependent molecular mechanisms regulating NK cell proliferation and cytotoxic function. Results of all experiments are outlined below.

SOW Task #1 To assess whether sustained miR-155 expression rescues NK cell killing of TKI-resistant quiescent leukemic stem cells (qLSCs)

1A) To assess *in vitro* miR-155 boosting effect on NK cell cytotoxicity against quiescent leukemic stem cells (LSCs).

- NK cells obtained from *lck-miR-155* C57BL/6 (miR-155-tg) and C57BL/6 (source of wt NK cells) mice were employed in cytotoxicity assays on CFSE-labeled lineage-negative (Lin^-) BM cells isolated from healthy (not-induced) and leukemic SCL-tTA-BCR-ABL1 (BCR-ABL1-tg; 8-12 week-induced). miR-155 expression markedly and significantly increased absolute numbers of BM NK1.1^+ and DX5^+ CD3^- cells (Fig. 1). Ectopic expression of miR-155 also significantly enhanced NK cell cytotoxic activity against quiescent (CFSE^{max}) leukemic $\text{Lin}^- \text{Sca}^+ \text{Kit}^+$ (LSK) stem cells (qLSCs) which were reduced by 50% upon exposure to miR-155-tg (miR-155-NK) NK (Fig. 2A).

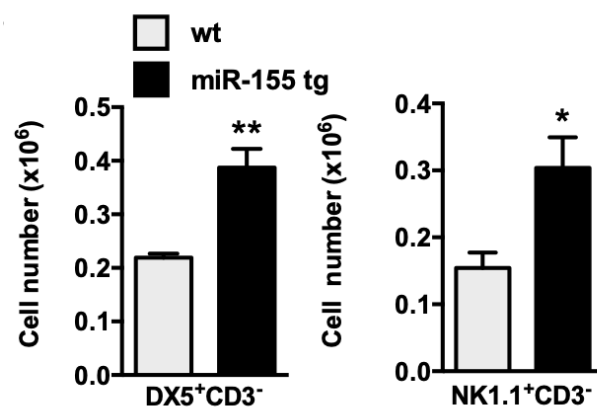


Fig. 1. Effects of miR-155 on NK cell numbers. Absolute DX5^+ (left) NK1.1^+ (right) CD3^- NK cell numbers in bone marrow of wild type (wt) and miR-155 transgenic (tg) mice. * $P < 0.05$, ** $P < 0.01$

- LTC-IC assays were performed as proposed according to the modified protocol reported in Ref. 77 of the funded grant. Unfortunately, no mouse LTC-IC colonies were obtained following such protocol; thus, to overcome this problem we assessed changes in LSC activity by determining the effect of wt and miR-155 tg NK cells on BCR-ABL1-tg LSK self-renewal in BM serial replating assays. In four independent experiments, miR-155 NK cells were significantly more efficient than wt NK cells to reduce mouse LSK replating efficiency (Fig. 2B) indicating that numbers of self-renewing long-term leukemic HSCs were more efficiently killed by miR-155 NK cells.
- As proposed, we counteracted miR-155 activity by lentiviral-mediated expression of SHIP-1. Results indicate that SHIP-1 significantly suppressed by ~50% NK cell-mediated killing of BCR-ABL⁺ cells (Fig. 2C)

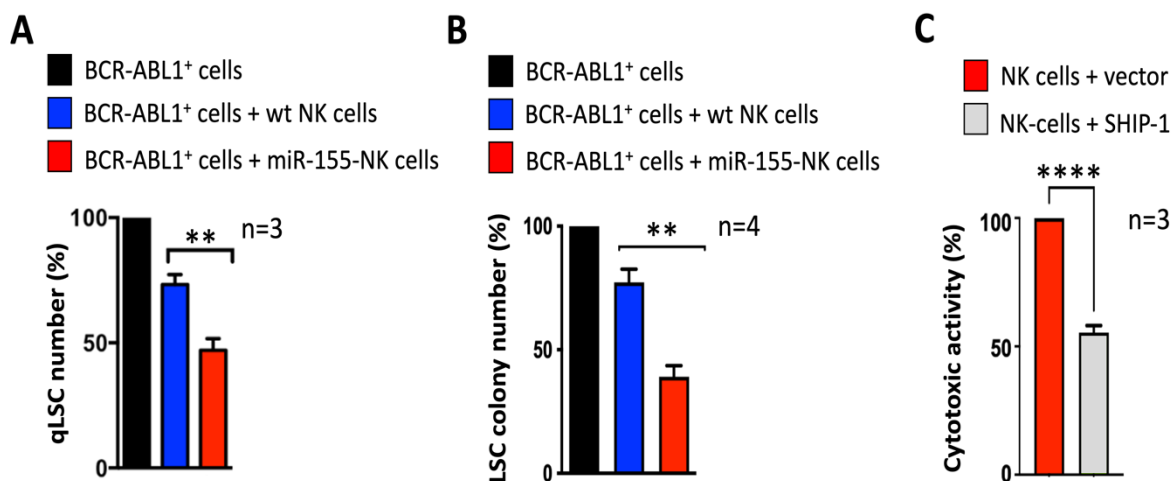


Fig. 2. Effects of miR-155 on NK cell cytotoxicity on BCR-ABL1⁺ qLSC numbers and LSC activity. (A): Spontaneous NK cell cytotoxicity toward CFSE-labeled SCL-tTA-BCR1-derived bone marrow BCR-ABL1⁺ qLSCs was determined by FACS-mediated evaluation of LSC numbers in Annexin V^{neg}CFSE^{max} cells before and after exposure to wild type (wt) and miR-155-tg NK cells for 18 hours. (B): Decreased methylcellulose serial replating efficiency of SCL-tTA-BCR1-derived LSCs (Lin⁺Sca1⁺Kit⁺) exposed for 18 hours to wt and miR-155-tg NK cells. (C) NK cell cytotoxic activity against BCR-ABL1⁺ cells upon forced expression of NK cell negative regulator and miR-155-target SHIP-1. ***P*<0.01, *****P*<0.0001.

1B) To determine whether miR-155 overexpression overcomes BMM (MSC and/or hypoxia)-induced suppression of human and mouse NK cell proliferation and cytotoxic activity.

- **Effect on NK cell proliferation.** Numbers of mouse wt but not miR-155-tg NK cells were strongly reduced (50% inhibition) upon 5-day exposure to M2104 murine BM MSC-CM, suggesting that miR-155 overexpression can overcome BM MSC-induced NK cell growth inhibition (Fig. 3A).

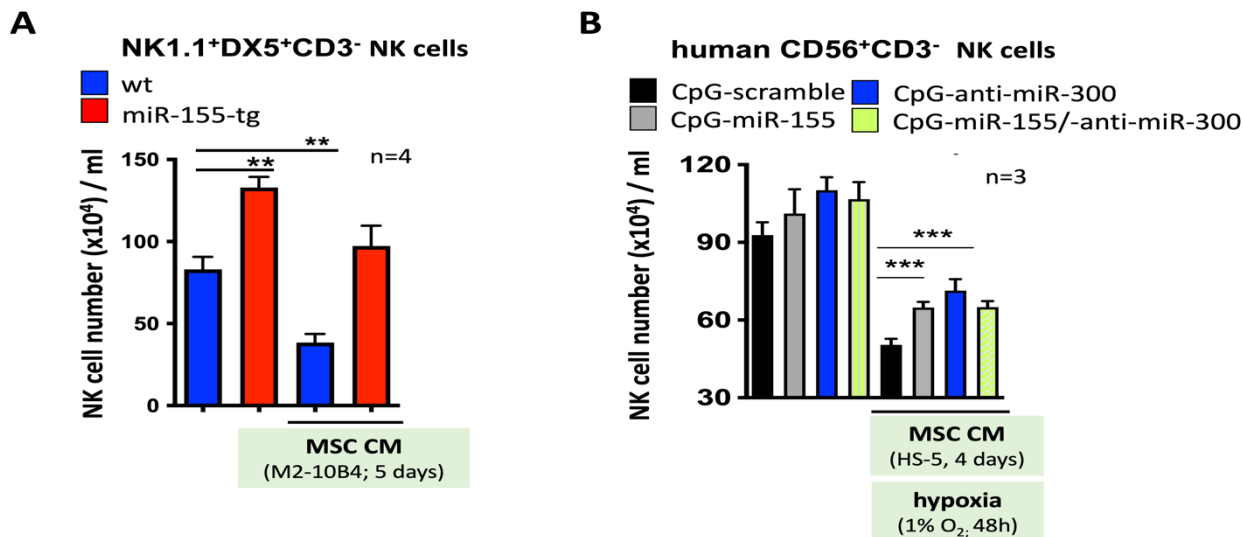


Fig. 3. Effects of miR-155 and/or anti-miR-300 on BMM-induced suppression of NK cell proliferation. (A): Effect of M2-10B4 mesenchymal stromal cell (MSC) conditioned medium (CM; 100% vol/vol) on wt and miR-155-tg NK cell proliferation after 5-day culture in presence of IL-2. (B): Effect of bone marrow HS-5 MSC CM and hypoxia on proliferation of human NK cells exposed to 500nM CpG-scramble, CpG-miR-155 and/or CpG-anti-miR-300. Results are expressed as the mean \pm SEM. ***P*<0.01, ****P*<0.001

BM mesenchymal stromal cell (MSC) conditioned medium (CM)-induced inhibition of NK-92 cell proliferation was ~30% and ~50% rescued by 500nm CpG-miR-155-5p and 500nM CpG-anti-miR-300 treatment, respectively, but neither additive nor synergistic effect was observed with the miR-155/anti-miR-300 combination (Fig. 3B).

- **Effect on NK cell cytotoxic activity.** Unexpectedly, treatment with CpG-miR-155-5p or CpG-anti-miR-300 did not overcome BM MSC HS-5 CM (100% vol/vol)- and hypoxia (1% O₂, 48h)-induced suppression of CD56⁺CD3⁻ NK-92 cell cytotoxic activity toward CML stem/progenitor cells (Fig. 4A) despite a) SHIP1 levels in NK-92 cells were, as expected, markedly reduced (~80% inhibition) by 500nM CpG-miR-155-5p treatment (insets in Fig. 4A); and b) NK-92 cells efficiently killed (30-70% cytotoxic activity at E:T=10:1) CD34⁺ CML qLSCs (*see fig. 4 in funded grant application*) and/or dividing CD34⁺ stem/progenitors isolated from 3 CML and AML BM samples (Fig. 4B, compare black to red bars). This suggests that augmenting levels of mature miR-155 with synthetic CpG-based oligonucleotides in NK cells is not sufficient to antagonize the combined inhibitory effect of hypoxia and MSCs on NK cell cytotoxic activity despite the ability of miR-155 to increase NK cell numbers in culture conditions mimicking the hypoxic leukemic stem cell BM niche (Fig. 3B).

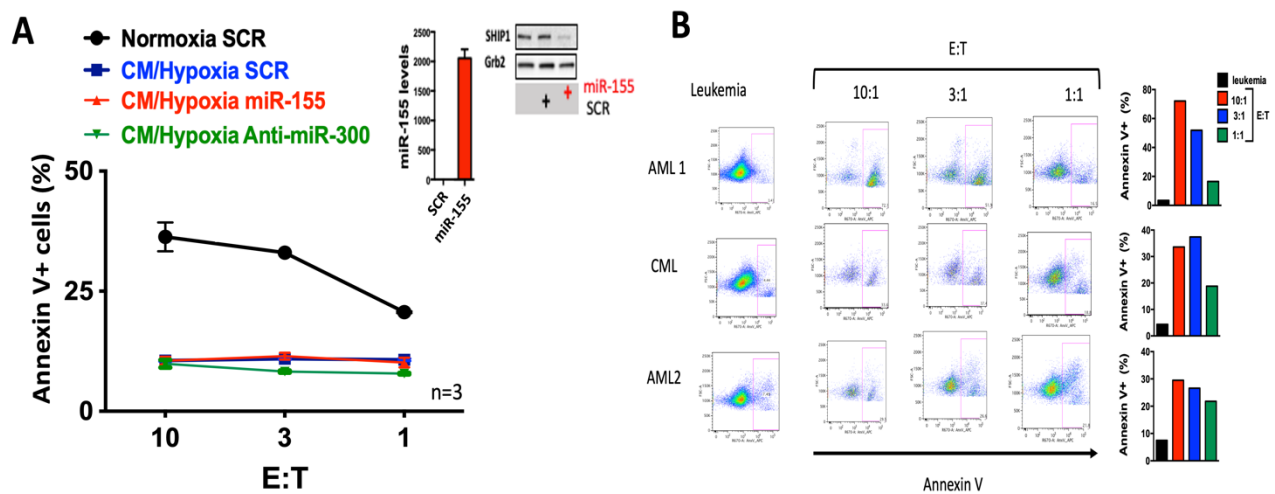


Fig. 4. Effects of miR-155 and/or anti-miR-300 on BMM-induced suppression of NK cell cytotoxicity. (A): Effect of 500nm CpG-scramble (SCR; control), CpG-miR-155 and CpG-anti-miR-300 on the cytotoxicity of human NK-92 cells against CD34⁺ CML stem/progenitor cells maintained in normoxic and hypoxic (1% O₂; 48 hours) conditions in MSC HS-5 conditioned medium. Graph shows the mean +/- SEM of Annexin V⁺ BCR-ABL1⁺ cells after exposure to NK cells at different E:T ratios. *Insets* show levels of miR-155 and of its direct target SHIP-1 in CpG-scramble and CpG-miR-155 treated cells. (B): Flow cytometry plots and relative graphs show the cytotoxic activity of human NK-92 cells (used at different E:T ratios) against primary CML and AML CD34⁺ stem/progenitor cells

SOW Task #2 To determine the *in vivo* therapeutic potential of miR-155-activated NK cell anti-LSC cytotoxic activity.

2A) Generation and *in vitro* functional characterization of BMM-resistant NK-92-155/anti-300 cells.

We have generated NK-92 cells expressing mature miR-155 and an anti-miR-300 and assessed changes in their activity toward BCR-ABL1⁺ cells. Results indicate that levels of ectopic mature miR-155 in these cells were not sufficient to augment NK cell cytotoxic activity toward BCR-ABL1⁺ K562 cells (Fig. 5A). Conversely, we found that overexpression of pre-miR-155, achieved by transducing NK-92 cells with lenti-pre-miR-155 (PMIRH155PA1; SBI System Bioscience), efficiently counteracted the MSC HS-5 CM inhibitory effect on NK cells and led to a >50% decrease in the

number of CML blast crisis (CML-BC; n=3) quiescent (eFluor^{max}CD34⁺) LSCs (qLSCs) and dividing CD34⁺ progenitors (Fig. 5B), suggesting that other mechanisms, which are counteracted by the expression of pre-miR-155, are responsible for the BMM-induced inhibition of NK cell cytotoxicity

2B) Assessing NK-92-155/300 cytotoxicity against CML qLSCs in CML mouse PDXs.

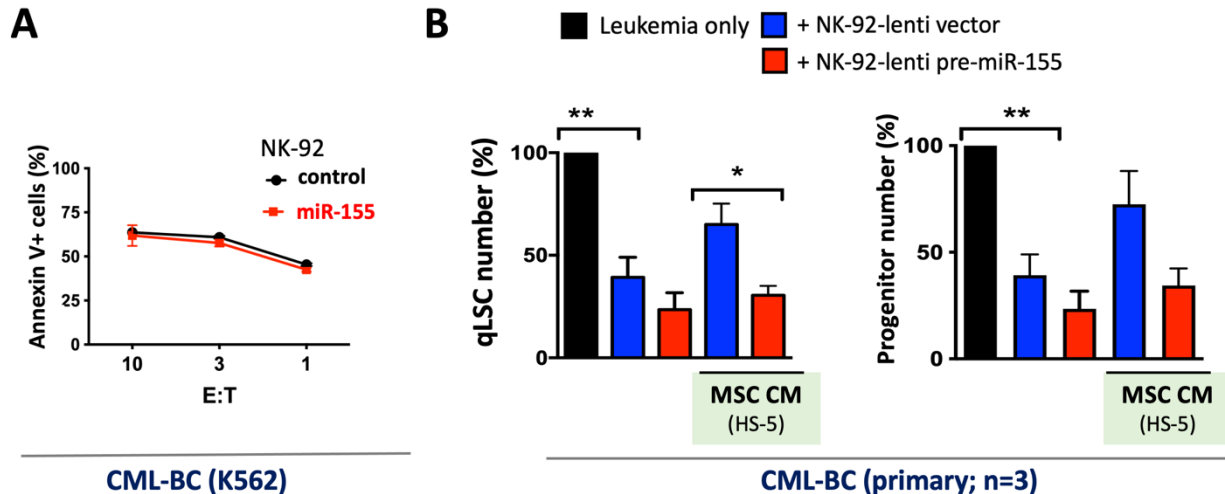


Fig. 5. Effects of ectopic mature miR-155 and pre-miR-155 expression on human CD56⁺CD3⁺ NK cell cytotoxicity. Cytotoxic activity against K562 CML-BC (A), primary CML-BC (n=3) CD34⁺ dividing progenitors (B right panel) and quiescent eFluor^{max}CD34⁺ LSCs (B left panel) of IL-2 cultured CD56⁺CD3⁺ NK-92 cells transduced with control vectors or with a construct containing a mature miR-155 (A) or a pre-miR-155 (B) cassette and IL-2 cultured in the presence or absence of MSC HS-5 conditioned medium (CM). Values represent the mean +/- SEM. *P<0.05, **P<0.01

Feasibility of these *in vivo* experiments was primarily precluded by the lack of mature miR-155 activity in human NK-92 cells.

As alternative experiments, **we followed the Reviewers' suggestions made to the funded grant application and assessed the mechanisms whereby pre-miR-155 and miR-300 regulate NK cell proliferation and/or cytotoxic activity against BCR-ABL1⁺ LSCs and progenitors.** Thus, we further investigated a) the effect of BMM (e.g. MSCs) on positive (e.g. SET) and negative (e.g. miR-300, CEBPB, SHIP-1) regulators of NK cell proliferation and cytotoxic activity in wild type and pre-miR-155-transduced NK cells; and determined b) whether altered FAS, DR5 and NKG2D ligands expression on BCR-ABL1⁺ LSK cells and FAS ligand and TRIAL levels on NK cells may account for the selective and enhanced LSC killing by ectopic pre-miR-155-expressing NK cells. Obtained results are outlined below.

- **BMM-induced miR-300-dependent molecular mechanisms regulating NK cell proliferation/activity.** We dissected the mechanism by which MSCs and hypoxia induces miR-300 to suppress NK cell growth and killing activity. We found that conditioned medium from both HS-5 and primary MSCs and hypoxia upregulated CEBPB expression (mRNA and protein) that, in turn, increased miR-300 levels and led to silencing of G1/S cell cycle regulators (i.e., CCND2 and CDK6) and PP2A inhibitor SET in NK cells. Moreover, we found that levels of pre-miR-155 were downregulated upon exposure of NK cells to MSC-derived exosomes (*these experiments have been reported in fig. 5 and S5 of the enclosed publication*). Because loss of CCND2/CDK6 activity arrests proliferation and SET inhibition (PP2A activation) impairs NK cell activation and cytotoxicity, miR-300-induced suppression of these factors may represent the mechanism by which the BMM suppresses NK cell growth and activity against LSCs.

- Interplay between MSC-induced and pre-miR-155-dependent molecular mechanisms regulating NK cell proliferation/activity.** We also found that GFP-sorted pre-miR-155-overexpressing NK-92 cells, maintained in the absence of IL-2, showed reduced SHIP-1 and increased SET expression (Fig. 6). This might explain the reported (Fig. 5B) ability of pre-miR-155 to rescue NK-92 cell spontaneous cytotoxicity toward qLSCs and CD34⁺ progenitors from CML patient samples from the inhibitory effects of BM MSCs. By contrast, levels of pri-miR-300 and those of its positive transcriptional regulator CEBPB were strongly induced by exposure to MSC HS-5 CM and insensitive to ectopic pre-miR-155 expression (Fig. 6). This suggests that miR-300 and pre-miR-155 are independent signals that negatively and positively, respectively, regulate NK cell proliferation and anti-leukemia cytotoxic activity although pre-miR-155-induced SET expression may, at least in part, counteract the MSC-induced CEBPB-miR-300-mediated SET downregulation (see enclosed publication).

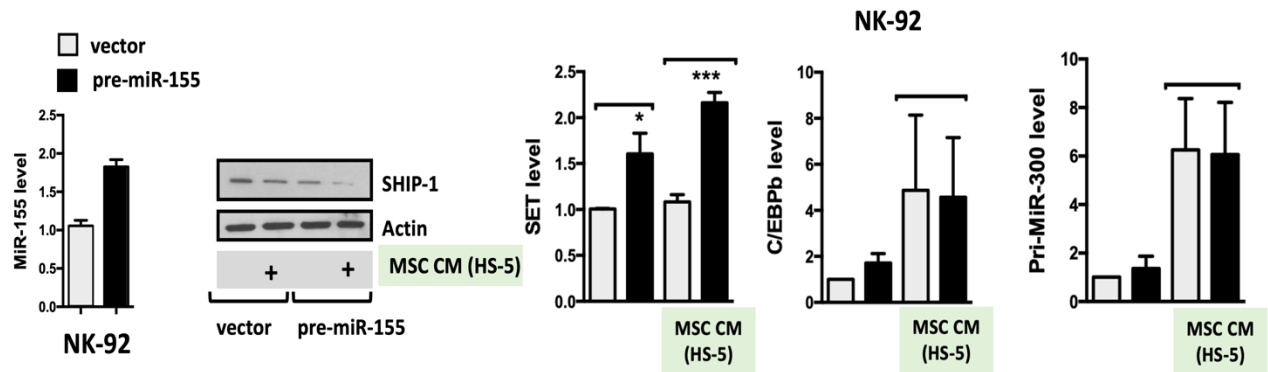


Fig. 6. Effects of ectopic pre-miR-155 expression of NK cell regulatory molecules. (Left to right): Expression of miR-155, SHIP-1 (western blot is representative of three independent experiments), SET, CEBPB and pri-miR300 in vector- and pre-miR-155-transduced, GFP-sorted and IL-2-cultured NK-92 cells in the absence or presence of MSC HS-5 CM (100% vol/vol). Results are expressed as the mean +/- SEM of n=3 experiments. * $P < 0.05$, *** $P < 0.001$

- Regulation of NK:leukemia cell interaction by miR-155.** We assessed levels of NK cell receptors and ligands and found that FAS and DR5 expression is significantly upregulated whereas levels of NKG2D ligands Rae1 and MULTI1 but not those of HS60 are barely detectable in leukemic LSKs (Fig. 7), suggesting that FAS and DR5 may render CML qLSCs more susceptible NK cell cytotoxic activity. Analysis of FAS Ligand and TRIAL expression in primary NK1.1⁺CD3⁻ NK cells revealed that TRIAL levels are higher in miR-155 tg compared to wt NK cells maintained in resting condition (Fig. 8A).

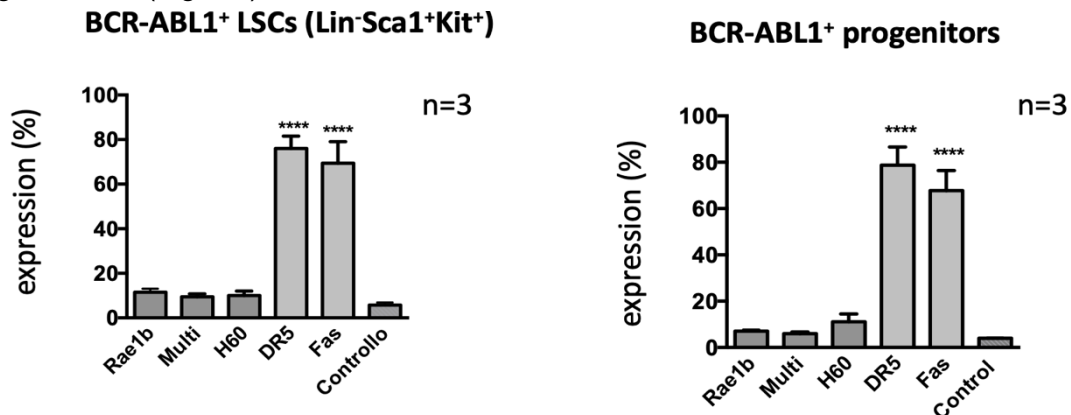


Fig. 7. Expression of NK cell receptors in mouse BCR-ABL⁺ cells. Levels of Rae1b, Multi, H60, DR5 and FAS in primary SCL-tTA-BCR/ABL-derived (n=3) bone marrow Lin⁻Sca1⁺Kit⁺ (LSCs) and Lin⁻Sca1⁺Kit⁺ (progenitors) cells. Results are expressed as the mean +/- SEM. **** $P < 0.0001$

Conversely, FAS Ligand and TRIAL expression was not significantly different in IL-2-cultured wt and miR155 tg NK1.1⁺CD3⁻ NK cells cultured in the absence or presence of mouse MSC CM (Fig. 8A). Consistent with the expression studies, wt and miR-155-tg NK cell-mediated cytotoxic activity against BCR-ABL1⁺ progenitors was FAS dependent but NKG2D independent (Fig. 8B).

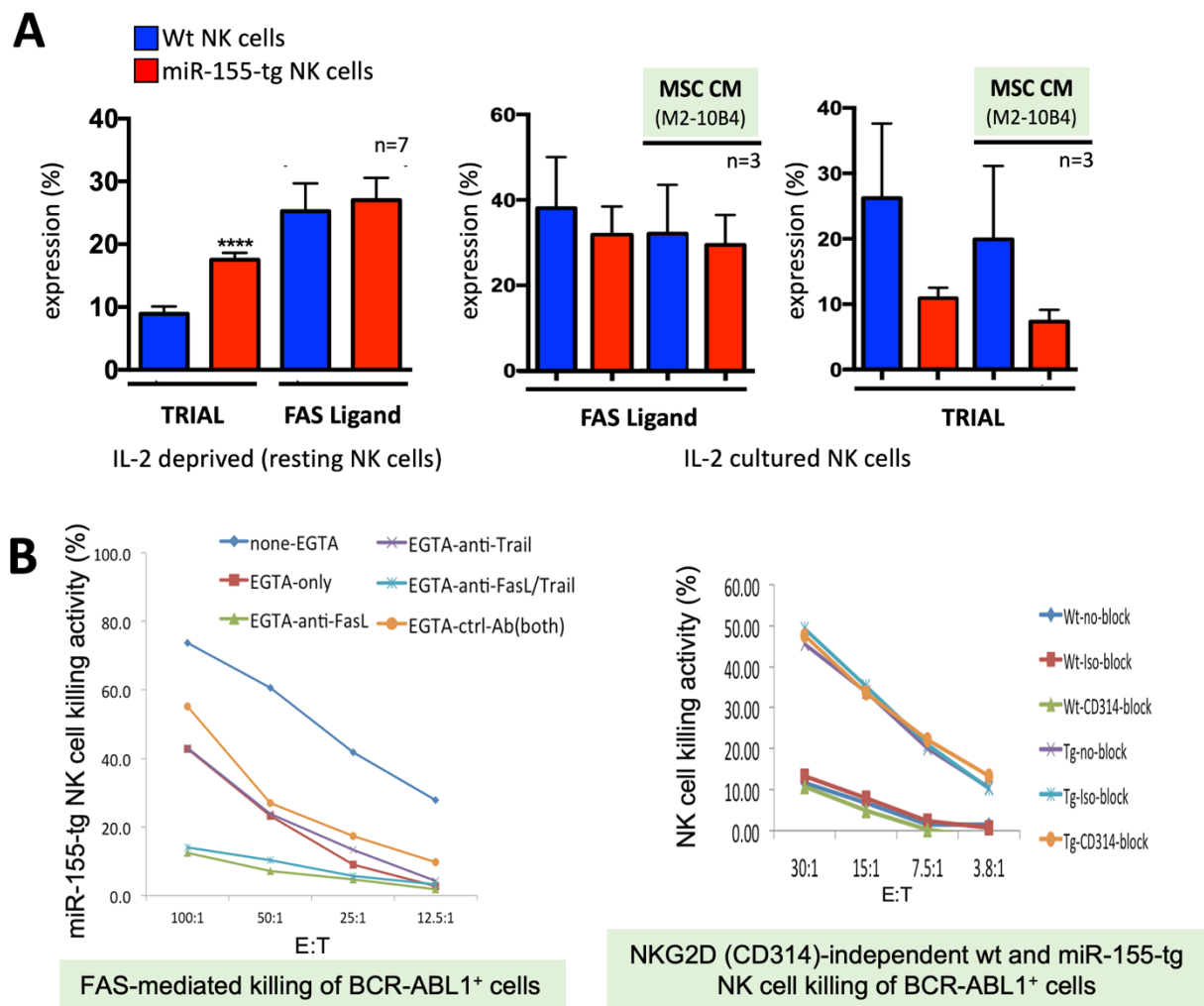


Fig. 8. Expression and role of FAS and TRIAL in wt and miR-155-tg NK cells. (A): Comparative analysis of FAS Ligand and TRIAL surface expression on splenic wt and miR-155-tg NK1.1⁺CD3⁻ NK cells analyzed after purification (resting) or after culturing in IL-2 +/- MSC HS-5 CM. Results are expressed as the mean +/- SEM. *****P*<0.000. (B) Cytotoxicity assays were performed in medium without or with 1mM EGTA/2mM MgCl₂ and anti-FAS Ligand or/and anti-TRAIL antibody or control antibody (left panel), or in the absence or presence of anti-NKG2D (CD314) block or isotype-matched (iso) control antibody block (right panel). 32D-BCR-ABL cells were used as targets. Effector cells were splenic NK1.1⁺CD3⁻ NK cells from wt and miR-155-tg mice. Results are from one representative experiment. x-axis, E:T cell ratio; y-axis, percentage of killing activity.

What opportunities for training and professional development has the project provided?

Nothing to report

How were the results disseminated to communities of interest?

Nothing to report

What do you plan to do during the next reporting period to accomplish the goals?

Nothing to report

4. IMPACT:

What was the impact on the development of the principal discipline(s) of the project?

Nothing to report

What was the impact on other disciplines?

Nothing to report

What was the impact on technology transfer?

Nothing to report

What was the impact on society beyond science and technology?

Nothing to report

5. CHANGES/PROBLEMS:

We found that the ability of miR-155 to enhance NK cell proliferation and cytotoxicity of NK1.1⁺CD3⁻ NK cells was not dependent on the activity of mature miR-155 only (as expected) but it required pre-miR-155 expression. Thus, we used a pre-miR-155 (lenti-pre-miR-155) instead of mature miR-155 for executing the proposed experiments.

Actual or anticipated problems or delays and actions or plans to resolve them

The in vivo experiments proposed in Aim 2B with human NK cells have been precluded by the evidence that NK-92 cells engineered to overexpress miR-155/anti-miR-300 (Aim 2A) did not confirm those obtained using miR-155 transgenic NK cells (Aim 1). Additional experiments (suggested by the Reviewers' panel) aimed at determining the molecular mechanisms regulating miR-155/miR-300-regulated ability of NK cells to kill leukemic cells were instead performed.

Changes that had a significant impact on expenditures

Nothing to Report.

Significant changes in use or care of human subjects, vertebrate animals, biohazards, and/or select agents

Significant changes in use or care of human subjects

Nothing to Report.

Significant changes in use or care of vertebrate animals

Although the NRG-SGM3 mouse colony was expanded to perform experiments described in Task 2B, the advent of COVID-19 pandemic obliged us to euthanize all mice. At the end of pandemic and in light of the new results (Fig. 5) , we arrived at conclusion that those experiments were not feasible because of the lack of effect of mature miR-155 on NK cell cytotoxic activity toward leukemic stem cells.

Significant changes in use of biohazards and/or select agents

Nothing to Report.

6. PRODUCTS:

- **Publications, conference papers, and presentations**

Journal publications.

Silvestri G.*, Trotta R.* Stramucci L., Ellis J., Harb J., Neviani P., Wang S., Eisfeld A.K., Walker C.J., Zhang B., Srutova K., Gambacorti-Passerini C., Pineda G., Jamieson CHM., Calabretta B., Stagno F., Vigneri P., Nteliopoulos G., May P., Reid A., Garzon R., Roy D.C., Moutouou M.M., Guimond M., Hokland P., Deininger M., Fitzgerald G., Harman C., Dazzi F., Milojkovic D., Apperley J.F., Marcucci G., Qi J., Machova-Polakova K., Zou Y., Fan X., Baer M. R., Calabretta B. and Perrotti D. *Persistence of drug-resistant leukemic stem cells and impaired NK cell immunity in CML patients depend on MIR300 anti-proliferative and PP2A-activating functions.* **Blood Cancer Discovery**. 1(1):48-67, 2020. (*) Co-first Authors

Books or other non-periodical, one-time publications.

Nothing to Report.

Other publications, conference papers and presentations.

Nothing to Report.

- **Website(s) or other Internet site(s)**

- <https://bloodcancerdiscov.aacrjournals.org>
- <https://twitter.com> (AACR Blood Cancer Discovery Twitter)

- **Technologies or techniques**

Nothing to Report.

- **Inventions, patent applications, and/or licenses**

Nothing to Report.

- **Other Products**

Nothing to Report.

7. PARTICIPANTS & OTHER COLLABORATING ORGANIZATIONS

What individuals have worked on the project?

Name: Danilo Perrotti

Project Role: PI

Researcher Identifier: ORCID ID: [0000-0003-0726-8766](#); [Scopus ID: 6603930319](#);

Nearest person month worked: 12

Contribution to Project: Conceptualization, formal data analysis, supervision, paper writing/editing. Funding Support: N/A

Name: Rossana Trotta

Project Role: Co-I

Researcher Identifier: ORCID ID [345462615](#); [Scopus ID: 7004543994](#)

Nearest person month worked: 12

Contribution to Project: Investigation, methodology, paper review and editing

Has there been a change in the active other support of the PD/PI(s) or senior/key personnel since the last reporting period?

Nothing to Report.

What other organizations were involved as partners?

Nothing to Report.

8. SPECIAL REPORTING REQUIREMENTS

COLLABORATIVE AWARDS:

QUAD CHARTS:

9. APPENDICES:

Persistence of Drug-Resistant Leukemic Stem Cells and Impaired NK Cell Immunity in CML Patients Depend on *MIR300* Antiproliferative and PP2A-Activating Functions

Giovannino Silvestri^{1,2}, Rossana Trotta^{2,3}, Lorenzo Stramucci^{1,2}, Justin J. Ellis^{4,5}, Jason G. Harb^{4,5}, Paolo Neviani^{4,5}, Shuzhen Wang¹, Ann-Kathrin Eisfeld^{4,5}, Christopher J. Walker^{4,5}, Bin Zhang⁶, Klara Srutova⁷, Carlo Gambacorti-Passerini⁸, Gabriel Pineda⁹, Catriona H. M. Jamieson¹⁰, Fabio Stagno¹¹, Paolo Vigneri¹¹, Georgios Nteliopoulos¹², Philippa C. May¹², Alistair G. Reid¹², Ramiro Garzon^{4,5}, Denis-Claude Roy¹³, Moutuaata M. Moutuou¹³, Martin Guimond¹³, Peter Hokland¹⁴, Michael W. Deininger¹⁵, Garrett Fitzgerald¹⁶, Christopher Harman¹⁶, Francesco Dazzi¹⁷, Dragana Milojkovic¹², Jane F. Apperley¹², Guido Marcucci⁶, Jianfei Qi², Katerina Machova Polakova⁷, Ying Zou², Xiaoxuan Fan², Maria R. Baer^{1,2}, Bruno Calabretta¹⁸, and Danilo Perrotti^{1,2,12,19}

ABSTRACT

Persistence of drug-resistant quiescent leukemic stem cells (LSC) and impaired natural killer (NK) cell immune response account for relapse of chronic myelogenous leukemia (CML). Inactivation of protein phosphatase 2A (PP2A) is essential for CML-quiescent LSC survival and NK cell antitumor activity. Here we show that *MIR300* has antiproliferative and PP2A-activating functions that are dose dependently differentially induced by CCND2/CDK6 and SET inhibition, respectively. *MIR300* is upregulated in CML LSCs and NK cells by bone marrow microenvironment (BMM) signals to induce quiescence and impair immune response, respectively. Conversely, BCR-ABL1 downregulates *MIR300* in CML progenitors to prevent growth arrest and PP2A-mediated apoptosis. Quiescent LSCs escape apoptosis by upregulating *TUG1* long noncoding RNA that uncouples and limits *MIR300* function to cytostasis. Genetic and pharmacologic *MIR300* modulation and/or PP2A-activating drug treatment restore NK cell activity, inhibit BMM-induced growth arrest, and selectively trigger LSC apoptosis *in vitro* and in patient-derived xenografts; hence, the importance of *MIR300* and PP2A activity for CML development and therapy.

SIGNIFICANCE: Tumor-naïve microenvironment-induced *MIR300* is the only tumor suppressor miRNA that induces CML LSC quiescence while inhibiting NK cell antitumor immune response and CML LSC/progenitor cell apoptosis through its anti-proliferative and PP2A-activating functions, respectively. Thus, the importance of *MIR300* and PP2A-activating drugs for formation/survival and eradication of drug-resistant CML LSCs, respectively.

¹Department of Medicine, University of Maryland School of Medicine, Baltimore, Maryland. ²Marlene and Stewart Greenebaum Comprehensive Cancer Center, University of Maryland School of Medicine, Baltimore, Maryland. ³Department of Microbiology and Immunology, University of Maryland School of Medicine, Baltimore, Maryland. ⁴Department of Molecular Virology Immunology and Medical Genetics, The Ohio State University Comprehensive Cancer Center, Columbus, Ohio. ⁵Department of Internal Medicine, The Ohio State University Comprehensive Cancer Center, Columbus, Ohio. ⁶Division of Hematopoietic Stem Cell and Leukemia Research, City of Hope National Medical Center, Duarte, California. ⁷Institute of Hematology and Blood Transfusion, University of Prague, Prague, Czech Republic. ⁸Hematology and Clinical Research Unit, San Gerardo Hospital, Monza, Italy. ⁹Department of Health Sciences, School of Health and Human Services, National University, San Diego, California. ¹⁰Department of Medicine and Moores Cancer Center, University of California, San Diego, La Jolla, California. ¹¹Division of Hematology and Unit of Medical Oncology, A.O.U. "Policlinico-Vittorio Emanuele", University of Catania, Catania, Italy. ¹²Department of Haematology, Hammersmith Hospital, Imperial College London, London, United Kingdom. ¹³Department of Hematology and Cellular Therapy Laboratory, Hôpital Maisonneuve-Rosemont, University

of Montreal, Montreal, Quebec, Canada. ¹⁴Department of Hematology, Aarhus University Hospital, Aarhus, Denmark. ¹⁵Division of Hematology and Hematologic Malignancies and Huntsman Cancer Institute, University of Utah, Salt Lake City, Utah. ¹⁶Center for Advanced Fetal Care University, University of Maryland School of Medicine, Baltimore, Maryland. ¹⁷Division of Cancer Studies, Rayne Institute, King's College London, London, United Kingdom. ¹⁸Sidney Kimmel Cancer Center, Thomas Jefferson University, Philadelphia, Pennsylvania. ¹⁹Department of Biochemistry and Molecular Biology, University of Maryland School of Medicine, Baltimore, Maryland.

Note: Supplementary data for this article are available at Blood Cancer Discovery Online (<https://bloodcancerdiscov.aacrjournals.org>).

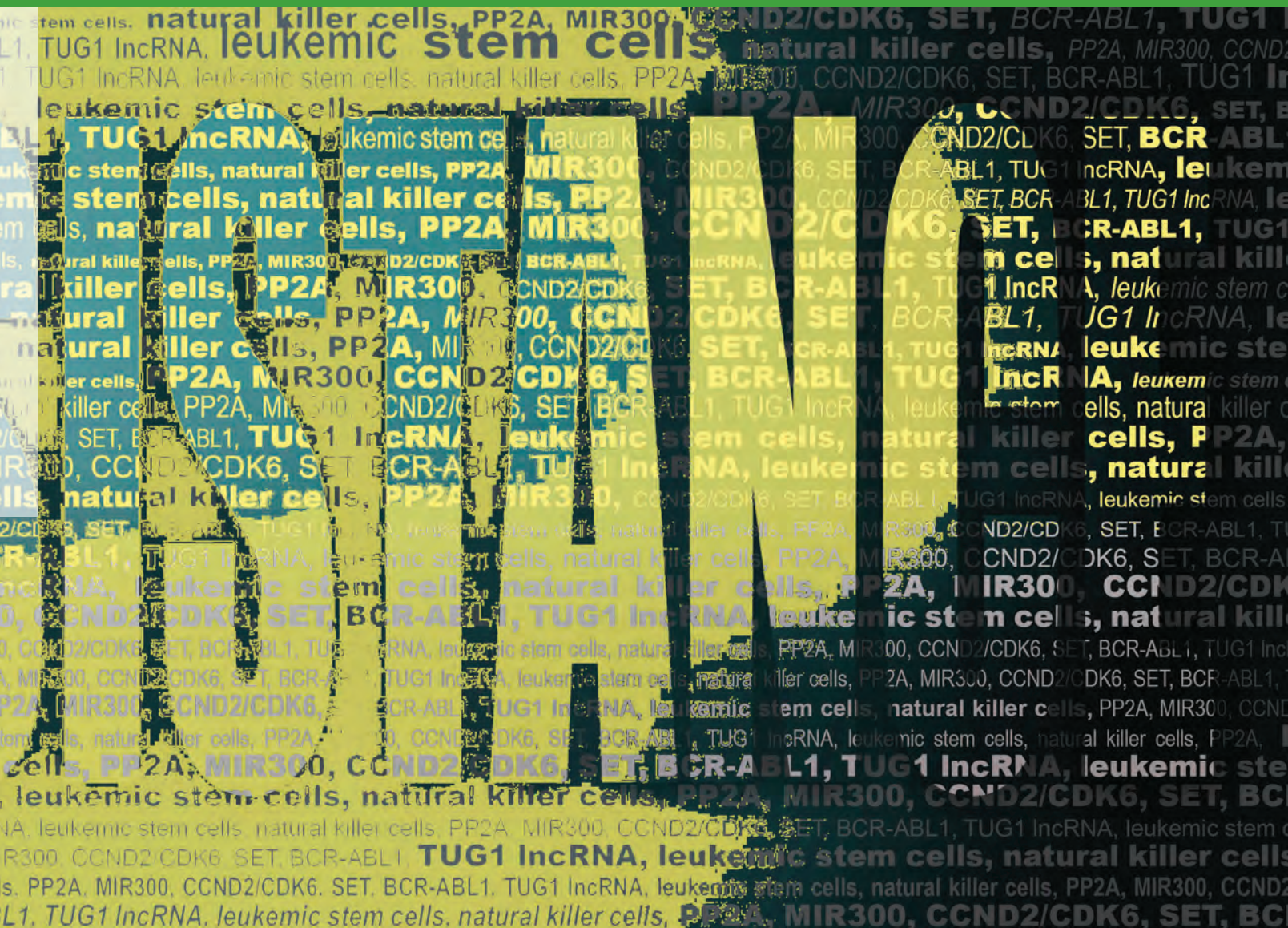
G. Silvestri and R. Trotta contributed equally to this article.

Corresponding Author: Danilo Perrotti, University of Maryland, 655 W. Baltimore St., Room 8-045, Baltimore, MD 21201. Phone: 267-968-4562; E-mail: dperrotti@som.umaryland.edu

Blood Cancer Discov 2020;1:1–20

doi: 10.1158/0008-5472.BCD-19-0039

©2020 American Association for Cancer Research.



INTRODUCTION

Chronic myeloid leukemia (CML) is a biphasic hematopoietic stem cell (HSC) myeloproliferative disorder driven by BCR-ABL1 oncogenic kinase activity (1). Despite being clinically manageable, CML is not a curable cancer and resistance to ABL tyrosine kinase inhibitors (TKI) remains a major therapeutic challenge (2). In fact, persistence of CML-initiating quiescent leukemic stem cells (qLSC) likely depends on their innate and acquired TKI resistance (3) and on impaired natural killer (NK) cell cytotoxicity against leukemic stem cells (LSC) (4), and accounts for disease relapse and dismal outcome (1, 5). Clinical trials, aimed at targeting intrinsic mechanisms of TKI resistance, failed to eradicate the TKI-resistant qLSC reservoir, likely because of bone marrow (BM) microenvironment (BMM) protective and inhibitory effects on LSCs and NK cells, respectively (5, 6).

Protein phosphatase 2A (PP2A) serine-threonine phosphatase is a druggable multimeric tumor suppressor inactivated in nearly all types of cancer, mostly by increased endogenous inhibitor (e.g., SET, CIP2A) or impaired subunit expression/function (7). PP2A loss-of-function is essential for cancer stem cell maintenance, tumor growth/progression, and activation of NK cell proliferation and antitumor cytotoxic activity (7). BCR-ABL1-independent and -dependent signals inhibit PP2A activity in CML [chronic (CP) and blastic (BC) phase] TKI-resistant qLSCs and TKI-sensitive and -resistant proliferating blasts, respectively, through activation of the SET-dependent PP2A inhibitory pathway (PIP; refs. 8, 9). Preclinical studies aimed at restoring physiologic PP2A activity with SET-sequestering PP2A-activating drugs (PADs; e.g., FDA-approved FTY720, OSU-2S, and OP449) have shown unprecedented antileukemia effects in TKI-sensitive

and -resistant CP and BC phase CML qLSCs and progenitors with neither adverse effects on normal hematopoiesis nor organ toxicity (8–10). In contrast, PP2A inhibiting drugs (PIDs; e.g., LB100), alone and in combination with TKIs, arrest proliferation of TKI-resistant CML progenitors, but do not exert effects on qLSC survival, and enhance leukemogenesis when used alone (11, 12).

The mechanisms underlying CML LSC quiescence, survival and self-renewal, and reduced NK-cell number and cytotoxicity likely result from integration of CML cell-autonomous and BMM-generated signals (1, 6). The latter are triggered by BM niche-specific metabolic conditions (e.g., oxygen tension), cell-to-cell direct, and soluble and/or exosome-encapsulated factor [e.g., microRNA (miRNA)]-mediated interactions between leukemic, mesenchymal stromal (MSC), endothelial, and immune cells (13–15).

Several miRNAs have been associated with PP2A inactivation (16) and LSC expansion and maintenance (17, 18); however, a clear causal link between their altered expression, persistence of drug-resistant LSCs, and PP2A loss-of-function is still missing.

Among the miRNAs predicted *in silico* to reactivate PP2A by targeting PIP factors (e.g., JAK2, hnRNPA1, and SET), we focused on hsa-miR-300 (*MIR300*), an intergenic miRNA that is inhibited in several stem cell-driven tumors and belongs to the 14q32.31 *DLK1-DIO3* genomic-imprinted tumor suppressor miRNA cluster B (19). Here we report that *MIR300* is a BMM-induced cell context-independent tumor suppressor with antiproliferative and PP2A-activating functions that are not only essential for induction and maintenance of LSC quiescence and impaired NK cell anticancer immunity, but they can also be exploited to selectively and efficiently induce PP2A-mediated cell death of CD34⁺ CML-quiescent

LSCs and proliferating progenitors while sparing normal hematopoiesis.

RESULTS

MIR300 Loss in Leukemic Progenitors and Differential Induction of Its Cell Context-Independent Tumor Suppressor Activities in TKI-Resistant Quiescent CML (CP and BC) LSCs

MIR300 levels were progressively and markedly reduced by BCR-ABL1 activity (imatinib treatment) in bulk and dividing BM CD34⁺ CML (CP and BC) progenitors compared with normal CD34⁺ BM (NBM) and umbilical cord blood (UCB) cells, and higher in HSC-enriched CD34⁺CD38⁻ than committed CD34⁺CD38⁺ CML (CP and BC) BM cells (Fig. 1A). Accordingly, *MIR300* expression was up to 800-fold lower in dividing CD34⁺ progenitors than qLSCs (CD34⁺CFSE^{max}) from patients with CML (CP and BC), but similar in quiescent and proliferating CD34⁺ UCB (Fig. 1B) cells.

Restoring *MIR300* expression at physiologic levels by CpG-based oligonucleotides (500 nmol/L CpG-miR-300) reduced $\geq 75\%$ proliferation and clonogenic potential and enhanced apoptosis (spontaneous and TKI-induced) of CD34⁺ CML (CP and BC), but not UCB cells (Fig. 2A and B). Importantly, Ki-67/DAPI and FUCCI2BL-mediated cell-cycle analyses in CD34⁺ CML and LAMA-84 cells, respectively, indicated that *MIR300* arrested cell cycle and markedly expanded qLSC (G0 $\cong 50\%$) and apoptotic sub-G₁ cell fractions of CML, but not normal CD34⁺ cells (Fig. 2C).

Inhibition of *MIR300* function (500 nmol/L CpG-anti-miR-300) did not reduce numbers [carboxyfluorescein diacetate succinimidyl diester (CFSE) assay] and clonogenic activity [colony forming cells (CFC) and/or long term culture-initiating

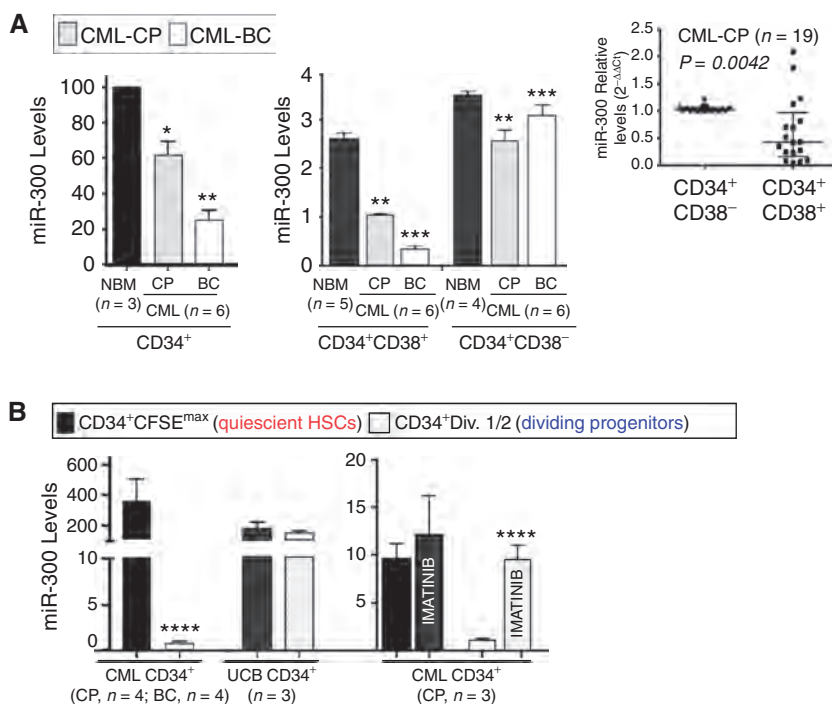


Figure 1. *MIR300* loss in leukemic progenitors and differential induction of its cell context-independent tumor suppressor activities in quiescent LSCs. **A**, (left) *MIR300* levels in healthy NBM and CML-CP and -BC CD34⁺ BM cell fractions. Inset shows *MIR300* levels in additional CD38⁻ fractionated CD34⁺ CML-CP BM cells expressed as n-fold difference in CD34⁺CD38⁺ compared with CD34⁺CD38⁻ samples. **B**, *MIR300* levels in untreated and imatinib (24 hours)-treated CD34⁺ quiescent (CFSE^{max}) and dividing (Div.1) CFSE-labeled CML and UCB cells. Asterisk on CD34⁺CD38⁻ cell populations (panel 1a) indicate significance between *MIR300* levels CD34⁺CD38⁻ versus CD34⁺CD38⁺ cells. Data are shown as mean \pm SEM from at least three independent experiments; *, $P < 0.05$; **, $P < 0.01$; ***, $P < 0.001$; ****, $P < 0.0001$.

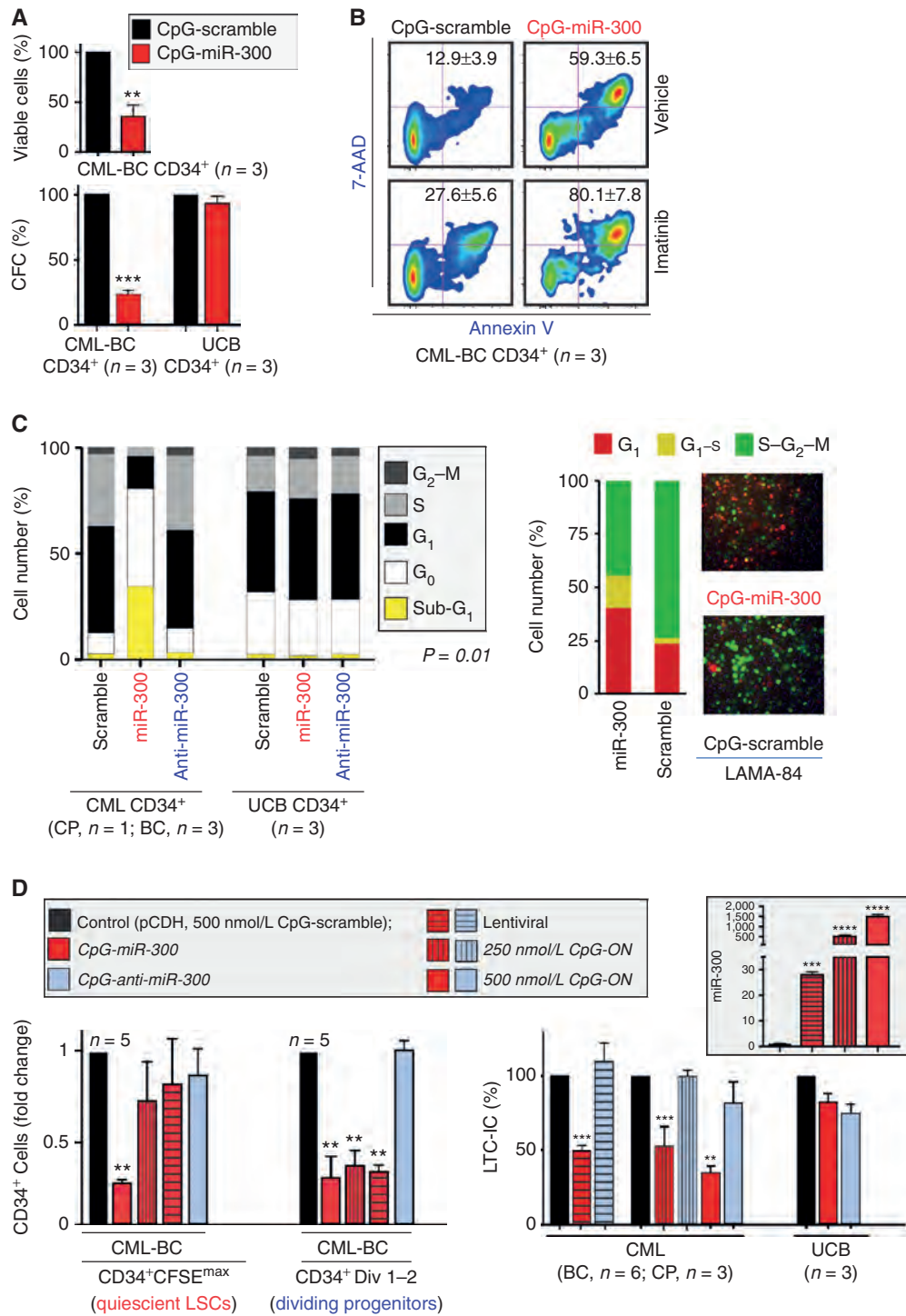


Figure 2. *MIR300* activity in quiescent leukemic stem and progenitor cells. **A**, Growth (48 hours) and clonogenic potential (CFC) of CpG-scramble- and CpG-miR-300-treated (500 nmol/L) CD34⁺ CML-BC and UCB cells. **B**, Effect of CpG-miR-300 and CpG-scramble (500 nmol/L) on spontaneous and IM (18 hours)-induced apoptosis (Annexin V/7-AAD) in CD34⁺ CML-BC cells (n = 3). Data are reported as mean ± SE (P < 0.01) from three independent experiments inside representative Annexin V/7-AAD FACS pseudocolor plots. **C**, Ki-67/DAPI (left; G₀: *MIR300* ≅ 46% vs. scr ≅ 10%; G₁: *MIR300* ≅ 15% vs. scr ≅ 50%; S/G₂-M: *MIR300* ≅ 4% vs. scr ≅ 27.4%; and sub-G₁: *MIR300* ≅ 35% vs. scr ≅ 3%) and FUCCI-2BL (right; G₁-G₀: *MIR300* ≅ 40.2% vs. scr ≅ 23.6%; G₁-S: *MIR300* ≅ 15% vs. scr ≅ 2.85%; S/G₂-M: *MIR300* ≅ 45% vs. scr ≅ 76.6%) cell-cycle analysis of UBC and Ph⁺ (primary CD34⁺ and synchronized LAMA-84) cells exposed to the indicated CpG-ONs. **D**, Dose-dependent differential regulation of *MIR300* antiproliferative and proapoptotic activities on CML qLSC (CFSE^{max}) and progenitor (Div. 1-2) cell (left) and LTC-IC (right) numbers. Vector transduced and 500 nmol/L CpG-scramble and CpG-anti-miR-300 served as controls. Inset, *MIR300* levels in pCDH-*MIR300* lentiviral-transduced and 250-500 nmol/L CpG-miR-300-treated Ph⁺ cells. Data are shown as mean ± SEM from at least three independent experiments; *, P < 0.05; **, P < 0.01; ***, P < 0.001; ****, P < 0.0001. Range values of controls are reported in Supplementary Table S1.

cells (LTC-IC) of CML and normal CD34⁺ stem and progenitor cells (Fig. 2D; Supplementary Fig. S1). In contrast, graded ectopic *MIR300* expression (Fig. 2D, inset) differentially affected leukemic, but not UCB-quiescent stem cell activity and survival. In fact, low *MIR300* levels (pCDH-*MIR300* and 250 nmol/L *CpG-miR-300*) strongly inhibited CML (CP and BC) LTC-IC and/or CFC/replating activities without affecting qLSC numbers, whereas high *MIR300* doses (500 nmol/L *CpG-miR-300*) also reduced by more than 80% CML qLSCs and dividing CD34⁺ progenitor cell numbers (Fig. 2D; Supplementary Fig. S1). Thus, *MIR300* functions as a cell context-independent dual activity (antiproliferative and proapoptotic) tumor suppressor that inhibits LTC-IC-driven colony formation by impairing qLSC ability to enter cycle and undergo cytokine-induced differentiation without affecting their survival, which is halted at higher *MIR300* expression levels.

***MIR300* Acts as Master PP2A Activator and Inhibitor of G₁-S Transition in CML LSCs and Progenitors**

Consistent with the absolute requirement of PP2A inhibition for CML, but not normal stem/progenitor cell proliferation and survival (9), gene ontology (GO) and Kyoto Encyclopedia of Genes and Genomes (KEGG) functional enrichment and clustering of *MIR300*-predicted and -validated (e.g., CTNNB1, CCND2, and Twist1; ref. 19) mRNA targets indicated that most of *MIR300* targets are also validated PP2A targets (Supplementary Fig. S2) and that *MIR300* antiproliferative and proapoptotic activities may result either from targeting SET that, in turn, induces PP2A-dependent inactivation of factors important for G₁-S cell-cycle transition (e.g., CCND2, CDK6) and survival (e.g., CTNNB1, JAK2, Twist1, and MYC) of CML qLSCs and progenitors, or from their direct inhibition by *MIR300* (Supplementary Figs. S2 and S3A). Accordingly, *CpG-miR-300*, but not *CpG-scramble*, reactivated PP2A and markedly reduced CCND2, CDK6, JAK2, hnRNPA1, SET, CTNNB1 (β-catenin), MYC, and Twist1 expression in primary CD34⁺ CML (CP and BC) progenitors and Philadelphia-positive (Ph⁺) cell lines, but not in normal CD34⁺ cells (Fig. 3A) in which PP2A has no proapoptotic activity (8, 20). Importantly, expression of *MIR300*-insensitive Flag-tagged *SET* mRNAs lacking the entire 3'UTR (Flag-SET) or just a region encompassing the high- and low-affinity *MIR300*-binding sites (Flag-Δ3'UTR-SET), but not that of full-length wild-type SET (Flag-wt3'UTR-SET), rescued Ph⁺ cells from *MIR300*-induced cell-cycle arrest and PP2A-dependent apoptosis (Annexin V⁺ cells; Fig. 3A, right).

***MIR300* Dual Activity Is Regulated in a Dose-Dependent Differential Target-Selection Manner**

Hierarchically clustering of *MIR300* predicted and validated targets based on integration of different algorithms, some of which also take into account levels of *MIR300* and of its targets in normal and leukemic BM cells (i.e., ComiR, CSmiRTar), positioned the G₁-S cell-cycle regulators CCND2 and CDK6 within the top 2% and SET within the 5% of *MIR300* targets, followed by JAK2, hnRNPA1, CTNNB1, and Twist1 clustering within the top 25%, and MYC in the lower

75% of *MIR300*-interacting mRNAs (Fig. 3C; Supplementary Fig. S3B). Notably, other regulators of G₁-S transition (e.g., CNNA2) and LSC cell-cycle reentry (e.g., Notch signaling) clustered together with CCND2 and CDK6, whereas *MIR300* targets, belonging to JAK-STATs, PI3K-Akt, Wnt, MAPK signaling pathways, and regulating CML (CP and BC) progenitor cell survival and expansion, ranked below SET and within the bottom 75% of *MIR300* target distribution (Supplementary Fig. S3B), suggesting that their *MIR300*-induced inactivation/downregulation is PP2A-mediated, occurs upon SET inhibition, and requires levels of *MIR300* higher than those necessary to inhibit CCND2 and CDK6 and trigger cell-cycle arrest in a PP2A-independent fashion. This implies that the differential induction of *MIR300* antiproliferative and proapoptotic activities (Fig. 2C and D) may depend on its ability to select targets in a dose-dependent manner. Indeed, low levels of ectopic *MIR300* expression, achieved by exposing CD34⁺ CML-BC stem/progenitor cells to *CpG-miR-300* concentrations (e.g., 100 nmol/L) not triggering qLSC apoptosis (Fig. 2D), strongly reduced CCND2 and CDK6, but not SET expression that, instead, became barely detectable at *CpG-miR-300* doses (e.g., 500 nmol/L) inducing qLSC apoptosis (Fig. 3B, right). This is also consistent with the presence of four, six, and two *MIR300*-binding sites in CCND2, CDK6, and SET mRNA 3'UTRs, respectively (Fig. 3B, left).

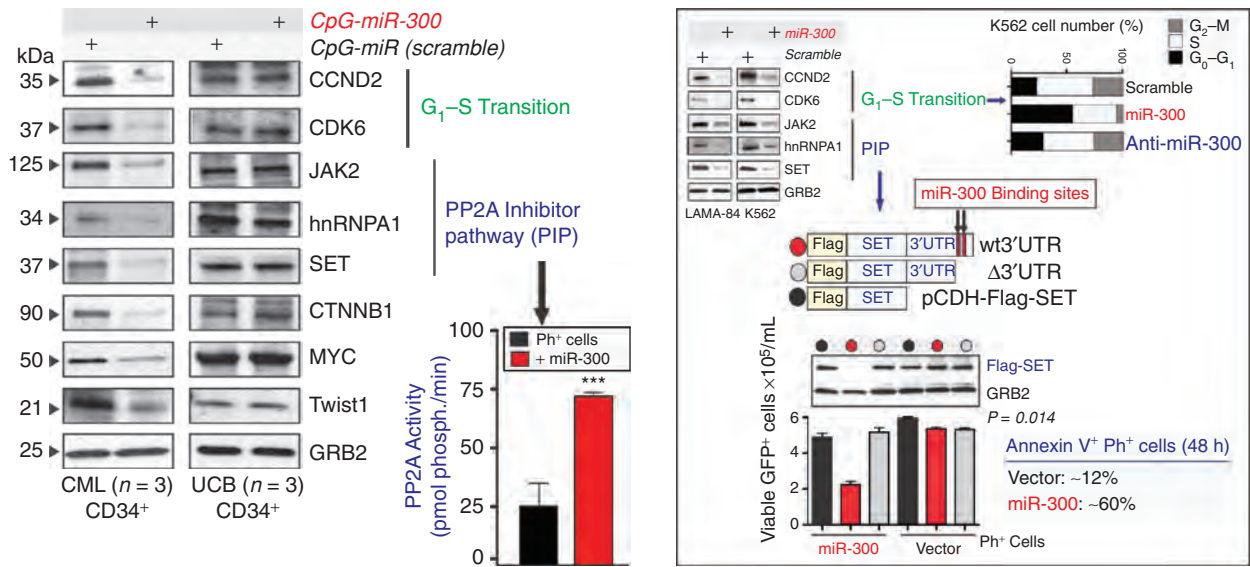
Because CDK6/CCND2 downregulation is an essential feature of G₁-G₀-arrested myeloid qLSCs (21, 22) and SET inhibition is sufficient for inducing PP2A-dependent CML LSC and progenitor cell apoptosis (8, 9), the ability of *MIR300* to sequentially trigger growth arrest and PP2A-mediated apoptosis of CD34⁺ CML (CP and BC) qLSCs and progenitors suggests that *MIR300* expression in LSCs may account for their entry into quiescence, whereas its downregulation in leukemic progenitors likely occurs to prevent apoptosis (Fig. 3B, right).

***MIR300* Antiproliferative Activity Accounts for BMM-Induced CML LSC Entry into Quiescence**

MIR300 is under the control of an intergenic differentially methylated region (IG-DMR) preceding and controlling the expression of maternally expressed genomic-imprinted MEG3 lncRNA and other DLK1-DIO3 miRNAs (Supplementary Fig. S4A) that are strongly inhibited upon promoter methylation in several types of cancer, including myeloid leukemias (23). Treatment with 5-Aza-2'-deoxycytidine (5-Aza) augmented by 10⁴-10⁵-fold *MIR300* expression in Ph⁺ cells (Supplementary Fig. S4B); however, nearly all cells underwent apoptosis after 24 hours, suggesting that *MIR300* upregulation in CML qLSCs unlikely depends on IG-DMR demethylation and expression of all 74-cluster B tumor suppressor miRNAs (Supplementary Fig. S4A). Thus, *MIR300* induction may depend on BM osteogenic niche factors (e.g., MSCs, hypoxia, TGFβ1), known to inhibit growth and induce quiescence of leukemic cells (13, 14).

Indeed, expression of *MIR300* increased at qLSC or higher levels (Fig. 1B) upon exposure of primary CD34⁺ CML-BC and/or LAMA-84 cells and BM-derived primary CD34⁺CD45⁺CD73⁺CD105⁺CD90⁺CD44⁺ hMSCs and HS-5 MSCs to hypoxia, suggesting that MSCs may also contribute to enhanced *MIR300* levels in qLSCs (Fig. 4A and B).

A



B

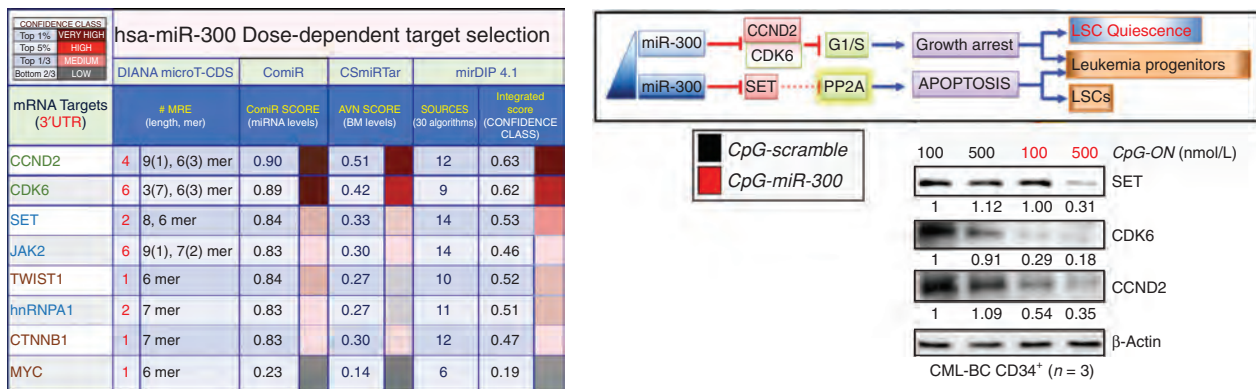


Figure 3. *MIR300* acts as master PP2A activator and inhibitor of G₁-S transition through a dose-dependent target selection mechanism. **A**, Left, representative blots show effect of *MIR300* on its targets and PP2A activity in UCB and CML-BC CD34⁺ cells and cell lines exposed to *CpG-scramble* and *CpG-miR-300* (500 nmol/L; 48–72 hours). Right, (top) Dapi/Ki67 cell-cycle analysis of *CpG-scramble*, *-miR-300*, and *CpG-anti-miR-300* (500 nmol/L; 21 hours)-treated aphidicolin-synchronized K562 cells; (middle) Flag-SET lentiviral constructs with wild-type or a deleted mRNA 3'UTR; (bottom) *MIR300*-induced downregulation of Flag-SET proteins, and rescue of Ph⁺ cells from exogenous *MIR300*-induced growth inhibition (Trypan blue exclusion)/apoptosis (Annexin V⁺) by Flag-SET cDNAs lacking *MIR300*-binding site. Similar results were obtained with LAMA-84 cells. **B**, Hierarchical clustering of statistically significant ($P < 0.05$ with FDR correction) *MIR300* targets using the indicated databases (number of binding sites is indicated in red). Top right, schematic representation of the biological effects of *MIR300* dose-dependent target selection activity in qLSCs and leukemic progenitors; (bottom) SET, CDK6, CCND2, and β -actin levels in *CpG-MIR300*- and *CpG-scramble*-treated (100–500 nmol/L; 48 hours) CML-BC CD34⁺ cells.

Accordingly, *MIR300* expression was strongly augmented in CD34⁺ CML cells exposed to hMSC and HS-5 conditioned medium (CM) and/or *MIR300*-containing CD63⁺Alix⁺ MSC exosomes (100 μ g/mL; Fig. 4C).

Hypoxia- and MSC-induced *MIR300* expression correlated with 40% to 60% reduced cell division and, importantly, with doubled numbers of cells in the CFSE^{max} CD34⁺ qLSC compartment (Fig. 4B and C; Supplementary Fig. S4C). Ph⁺ LAMA-84 cells also responded to MSC-CM exposure by ceasing proliferation and modifying gene expression (Supplementary Fig. S4D, left and right) in a manner similar to that of CML qLSCs (1). Importantly, exposure to MSCs (CM and/

or exosomes) neither diminished SET and PP2Ac^{Y307} (inactive) levels (Supplementary Fig. S4D, right) nor induced cell death (unchanged cell viability), suggesting that MSCs increase *MIR300* expression in CD34⁺ LSCs at levels sufficient to induce cell-cycle exit, but not to trigger PP2A-mediated apoptosis. Moreover, anti-*MIR300* molecules (*pZIP-miR-300* or *CpG-anti-miR-300*) suppressed hypoxia-induced *MIR300* target downregulation in CD34⁺ CML stem/progenitor cells and prevented MSC-induced inhibition of their proliferation when expressed in MSCs (Fig. 4A and C), further indicating that *MIR300* anti-proliferative activity likely mediates BMM-induced CD34⁺ LSC entry into quiescence in CML (CP and BC). Note that increased

β -catenin in HS-5 cells indicated functionality of lentivirally-transduced anti-*MIR300* construct (Fig. 4C, inset).

Hypoxia-Induced *MIR300* Expression in CML-BC LSCs Requires C/EBP β Activity

The notion that hypoxia induces quiescence of CD34⁺ CML LSCs and progenitors (24), and that hypoxia, but not MSCs, induces *MIR300*-dependent SET inhibition and increases levels of mature and primary (pri-miR-300) *MIR300* transcripts (Fig. 4A and D; Supplementary Fig. S4D) suggests that the contribution of hypoxia to *MIR300* expression in qLSCs is greater than that of MSC-derived exosomes, and that it may depend on increased *MIR300* transcription. Indeed, luciferase (luc) assays in normoxia- and hypoxia-cultured CD34⁺ CML-BC stem/progenitor cells transduced with reporter constructs containing full-length or 5'-deleted *MIR300* intergenic region revealed the presence of a hypoxia-sensitive regulatory element in the 109 bp preceding the human *MIR300* gene (Fig. 4E). ENCODE (V3) ChIP-Seq and PROMO analyses revealed that this 109 bp is located in a DNaseI hypersensitive region and contains two CCAAT Enhancer Binding Protein B (C/EBP β)-binding sites at position -64 and -46 that may drive transactivation of *MIR300* transcription. Site-directed mutagenesis of these C/EBP β -binding sites (p109mut) resulted in loss of luc activity (Fig. 4E), indicating that C/EBP β binding to this 109 bp regulatory element is essential for *MIR300* transactivation in hypoxia-, but not normoxia-cultured CD34⁺ CML-BC cells. Accordingly, increased pri-miR-300 expression correlated with markedly higher C/EBP β LAP1 (transcriptionally active) levels in hypoxic CD34⁺ CML-BC cells (Fig. 4D). In contrast, lack of C/EBP β -driven p109-luc activity in normoxic CD34⁺ CML-BC progenitors correlated with increased C/EBP β LIP (inhibitory function) expression (Fig. 4D). Consistent with the notion that *CEBPB* translation is inhibited by BCR-ABL1 activity (25) and that hypoxia inactivates BCR-ABL1 to induce LSC quiescence (14), *MIR300* induction by hypoxia was associated with decreased BCR-ABL1 activity, but not expression, (Fig. 4D) and ectopic C/EBP β -ER^{TAM} expression rescued primary (pri-miR-300) and mature *MIR300* expression in normoxic CD34⁺ CML-BC cells (Fig. 4F).

Hypoxia also substantially increased by 10- to 20-fold *MIR300* and C/EBP β protein, but not mRNA levels, in BM-derived primary MSCs and/or HS-5 cells (Fig. 4B; Supplementary Fig. S4E), suggesting that the hypoxic conditions of the osteogenic BM niche may increase *MIR300* levels in CML LSCs by simultaneously inducing C/EBP β LAP1-dependent *MIR300* transcription and increasing transfer of MSC-derived exosomal *MIR300*. Conversely, the evidence showing that *MIR300* levels in C/EBP β -responsive CD34⁺ CML-BC cells and/or Ph⁺ cell lines were not influenced by ectopic C/EBP α expression or exposure to TGF β 1-blocking antibody (Supplementary Fig. S4F and S4G), indicated that these qLSC regulators do not contribute to increased *MIR300* expression.

Notably, the notion that mouse *c/ebp β* induces BCR-ABL⁺ LSK exhaustion (26) does not argue against a role for human C/EBP β as an inducer of LSC quiescence because: (i) LSKs are pushed into cycle by constitutively activated BCR-ABL1 that promotes C/EBP β -dependent LSK maturation (26), (ii) the hypoxia-sensitive C/EBP β -responsive *MIR300* regulatory

element is not conserved in mouse cells, and (iii) an A-to-G substitution in mmu-miR-300 seed sequence at +4 position is predicted (miRTar, MFE: ≤ -10 kcal/mol; score: ≥ 136.5) to prevent mouse *MIR300* targeting of *ccnd2* and *cdk6* mRNAs.

MIR300 Is Upregulated in CML NK Cells and Its BMM-Induced Antiproliferative and PP2A-Activating Functions Impair NK Cell Immune Response

In CML, loss of NK cell antitumor immune response is causally linked to persistence of TKI-resistant LSCs (4, 27, 28). Cytotoxicity assays showed that cytokine-activated CD56⁺CD3⁻ NK cells can kill CD34⁺ CML-initiating qLSCs (Fig. 5A). Because cytokine-induced CCND2 expression and SET-dependent PP2A inhibition are essential for CD56⁺CD3⁻ primary NK and clinically relevant NK-92 cell proliferation and antitumor cytotoxicity (refs. 29, 30; Supplementary Fig. S5A), and KEGG/GO analyses predicted that *MIR300* regulates innate anticancer immunity (Supplementary Fig. S3A, right), we assessed whether reduced numbers and dysfunctional NK cells in patients with CML (28, 31) depend on increased *MIR300* expression.

MIR300 levels were increased in CD56⁺CD3⁻ NK cells from patients with CML at diagnosis, but not in NK cells, from healthy individuals (Fig. 5B), suggesting that loss of NK-cell proliferation and killing activity against CD34⁺ CML qLSCs and progenitors may depend on BMM-generated and leukemia-sustained *MIR300* antiproliferative and PP2A-activating functions. Indeed, exposure to hypoxia and BM MSC (primary hMSCs and HS-5 cells)-derived CM and/or Alix⁺CD63⁺ exosomes reduced by 45% to 75% IL2-dependent proliferation of CD56⁺CD3⁻ primary NK and NK-92 cells (Fig. 5C and D; Supplementary Fig. S5B) and severely impaired NK-cell immunoregulatory (IFN γ production) and anticancer cytotoxic (K562 killing) activities (Fig. 5E). Importantly, lentiviral anti-miR-300 (pZIP-miR-300) transduction into HS-5 cells and pretreatment of NK-92 cells with CpG-anti-miR-300, but not with CpG-scramble, significantly suppressed MSC CM- and/or exosome-inhibitory effects on NK cell proliferation and cytotoxicity against CML cells (Fig. 5D and E). Accordingly, IL2-induced proliferation and cytotoxicity of CD56⁺CD3⁻ NK and clinically relevant NK-92 cells was suppressed in CpG-miR-300-, but not CpG-scramble-treated cells (Fig. 5F), suggesting that impaired NK-cell growth and cytotoxicity against CML qLSCs and proliferating blasts occur in a *MIR300*-dependent manner through hypoxia- and MSC-(CM and exosomes) generated signals, increasing levels of C/EBP β and *MIR300* that, in turn, reduces CCND2, CDK6, and SET expression (Fig. 5C, E, and F).

Selective Suppression of *MIR300* Proapoptotic, But Not Antiproliferative Activity by *TUG1* lncRNA in CML Quiescent LSCs

Myeloid qLSCs display low to undetectable CCND2 and CDK6 expression, but high SET levels (9, 22, 32), and survive despite the high expression levels of a functional (target downregulation) *MIR300* (Figs. 1B and 4A), suggesting that a *MIR300*-interacting factor differentially regulates *MIR300* activities to prevent CML qLSC apoptosis while allowing LSC cell-cycle exit.

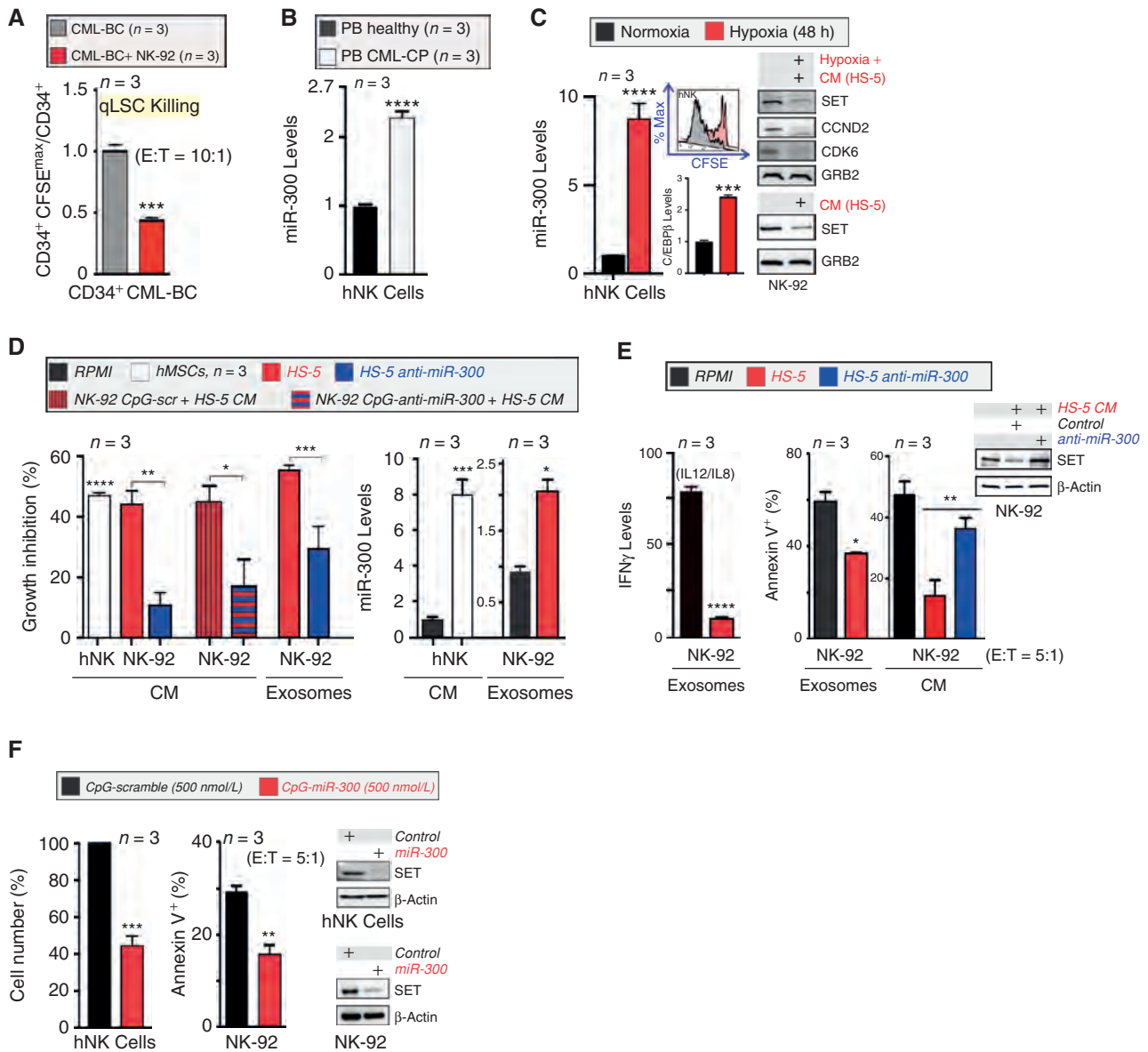


Figure 5. BMM-induced *MIR300* antiproliferative and PP2A-activating functions impair NK cell immune response. **A**, NK-92 cell cytotoxicity against CML-BC qLSCs. **B**, *MIR300* levels in $CD56^+CD3^-$ NK (hNK) cells from healthy and CML-CP individuals. **C**, Effect of hypoxia and MSC CM on *MIR300*, C/EBP β , SET, CCND2, CDK6, and GRB2 levels in hNK and/or NK-92 cells. Inset, effect of hypoxia on CFSE $^+$ NK cell growth. **D**, Effect of CM and exosomes from hMSCs and from parental, vector-, and anti-*MIR300*-transduced HS-5 cells on proliferation (left) and *MIR300* levels (right) in hNK and untreated, 500 nmol/L CpG-scramble or CpG-anti-*MIR300*-treated NK-92 cells. **E**, IL12/IL18 (18 hours)-induced IFN γ mRNA levels and NK cytotoxicity (% Annexin V $^+$ K562 cells) in IL2-cultured NK-92 cells exposed to CM or exosomes from parental or vector- and anti-*MIR300*-transduced HS-5 cells. Inset, SET and actin levels in NK-92 exposed to vector- and anti-miR300-transduced HS-5 CM. RPMI medium served as control. **F**, Effect of CpG-scramble and CpG-miR-300 treatment (500 nmol/L; 36 hours and 7 days) on IL2-depleted NK-92 cytotoxicity (% Annexin V $^+$ K562 cells), IL2-induced hNK cell proliferation (% cell number), and on SET and β -actin expression. Data are represented as mean \pm SEM for at least three experiments. Range values of controls are reported in Supplementary Table S1.

Because the taurine upregulated gene 1 (*TUG1*) is a *MIR300*-interacting (33) long noncoding RNA (lncRNA) that prevents the inhibition of *MIR300*-regulated factors (e.g., CCND1, CTNBN1, and Twist1) described as important for tumor cell growth and survival (34), we investigated whether *TUG1* may differentially regulate *MIR300* tumor suppressor activities in CML qLSCs (Fig. 6A).

TUG1 levels are markedly increased in $CD34^+CFSE^{max}$ CML qLSCs compared with dividing $CD34^+$ CML

progenitors and to $CD34^+CFSE^{max}$ UCB cells, but not in either $CD34^+CFSE^{max}$ UCB HSCs, compared with dividing $CD34^+$ UCB progenitors or $CD34^+$ Lin $^-$ compared with $CD34^+$ Lin $^+$ BM cells from healthy individuals (Fig. 6B; Supplementary Fig. S6A and S6B). In CML, *TUG1* is regulated in a manner similar to that of *MIR300*; in fact, *TUG1* expression is imatinib-insensitive in qLSCs, but not in dividing $CD34^+$ progenitors in which it is markedly suppressed by BCR-ABL1 activity (Fig. 6B).

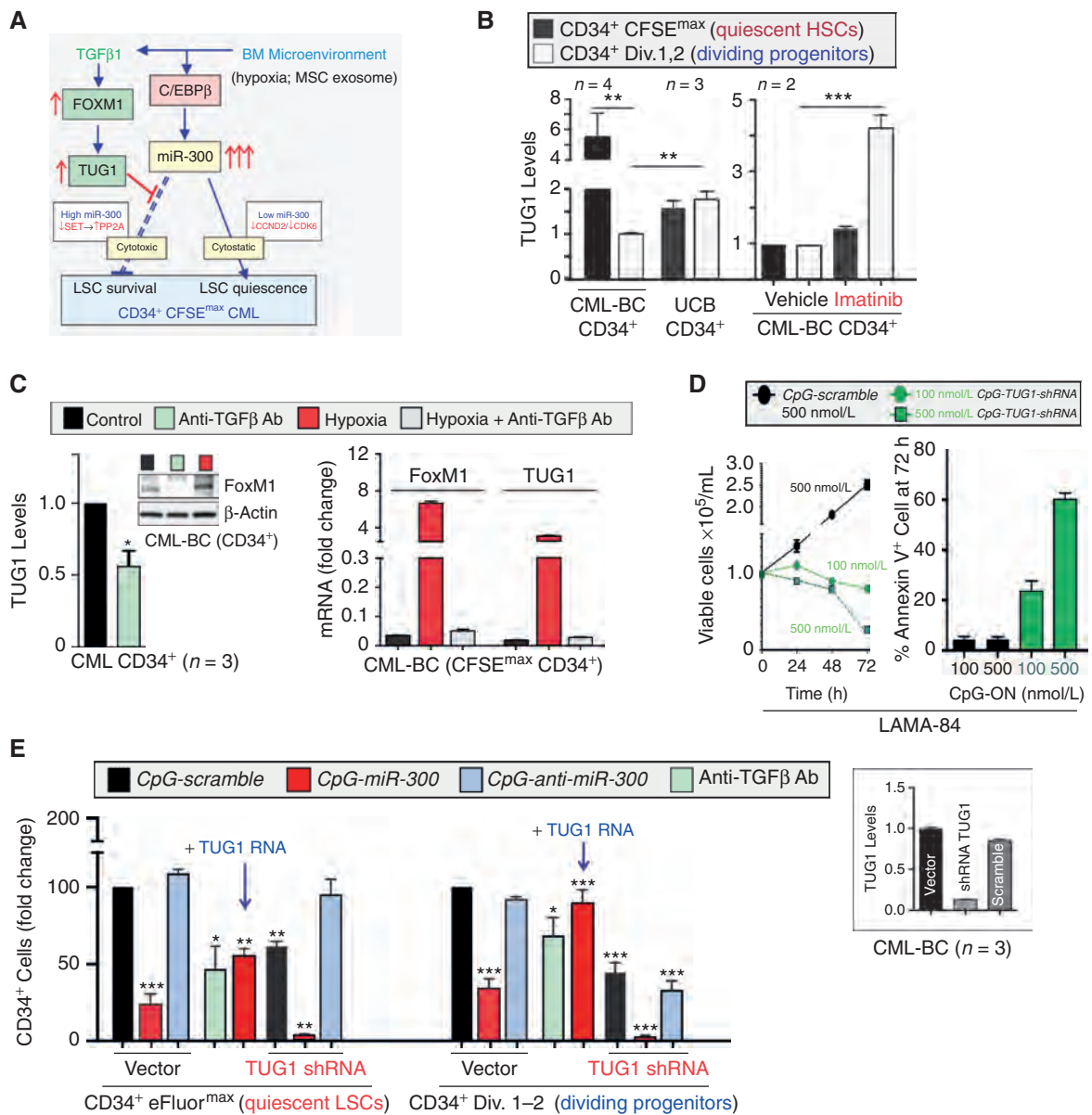


Figure 6. Selective suppression of *MIR300* proapoptotic, but not antiproliferative, activity by *TUG1* lncRNA in CML quiescent LSCs. **A**, BMM-generated signals regulating *MIR300-TUG1* interplay and its effect on CML LSC survival and quiescence. **B**, *TUG1* levels in CD34⁺ quiescent stem (CFSE^{max}) and dividing progenitors (Div.1, 2) and in untreated and imatinib-treated CD34⁺ CML cells. **C**, Effect of anti-TGFβ antibody (Ab) and/or hypoxia (1% O₂, 48 hours) on *TUG1* lncRNA and FoxM1 levels in CD34⁺ and CD34⁺CFSE^{max} CML-BC cells. **D**, Dose-dependent differential effect of low (100 nmol/L) and high (500 nmol/L) CpG-*TUG1*-shRNA and CpG-scramble on Ph⁺ LAMA-84 cell proliferation and survival (Annexin V). **E**, Effect of anti-TGFβ Ab, *TUG1*-shRNA, *TUG1* RNA, and control (CpG-scramble or empty vector) on recovery of untreated and CpG-scramble, -miR-300, and/or -anti-miR-300 eFluor^{max}CD34⁺ CML qLSCs (eFluor^{max}) and dividing (Div.1-2) progenitors relative to input. Inset, *TUG1* levels in vector, *TUG1* shRNA and scramble-shRNA cells. Data are represented as mean ± SEM for at least three experiments. Range values of controls are reported in Supplementary Table S1.

Because *TUG1* expression correlates with that of TGFβ1 in tumor cells (35) and TGFβ1 is a known inducer of LSC quiescence and it is secreted by leukemic cells including CD34⁺ CML blasts (36), we investigated the role of TGFβ1 in the regulation of *TUG1* expression and activity in CD34⁺ CML qLSCs and progenitors. Exposure (48 hours) of CD34⁺ CML-BC cells to a TGFβ1-blocking antibody (anti-TGFβ Ab; green bars) halves *TUG1* levels and also reduces levels of FoxM1 (Fig. 6C, left), a transcriptional factor that is

essential for quiescence and maintenance of hematopoietic stem cells, including CML LSCs, and induces *TUG1* expression in osteosarcoma cells (37–39). In contrast, FoxM1 and/or *TUG1* expression is strongly induced in a TGFβ-dependent manner in hypoxia-cultured (48 hours, 1% O₂) CML-BC CD34⁺CFSE^{max} and bulk CD34⁺ cells (Fig. 6C), suggesting that hypoxia-induced TGFβ1 (36) enhances *TUG1* levels in a FoxM1-dependent manner to neutralize *MIR300* proapoptotic activity in CML CD34⁺ qLSCs.

Indeed, dosing *TUG1* downregulation by exposure to low and high *CpG-TUG1-shRNA* concentrations mimicked the dose-dependent differential activation of *MIR300* antiproliferative and proapoptotic functions exerted by different *CpG-miR-300* doses (Fig. 2D); in fact, exposure of Ph⁺ cells (LAMA-84) to 100 nmol/L *CpG-TUG1-shRNA* efficiently induced growth arrest, but modestly affected survival (Annexin V⁺ cells; Fig. 6D and E, inset). Conversely, 500 nmol/L *CpG-TUG1-shRNA* decreased CD34⁺eFluor^{max} CML-BC qLSC and LAMA-84 cell numbers in a *MIR300*-sensitive manner and further enhanced *CpG-miR-300*-driven apoptosis resulting in a nearly complete loss of CD34⁺eFluor^{max} qLSCs and dividing CD34⁺ leukemic progenitors (Fig. 6D and E). As expected, exposure (48 hours) to a TGFβ1-blocking antibody markedly decreases qLSC numbers, but very modestly affects dividing leukemic progenitors (Fig. 6E). In contrast, *TUG1* overexpression (*TUG1 RNA*) antagonized *CpG-miR-300*-induced qLSC and progenitor cell apoptosis (Fig. 6E). *CpG-anti-miR-300* fully prevented *TUG1-shRNA*-induced apoptosis of CML CD34⁺eFluor qLSCs (Fig. 6E), suggesting that CML LSC entry into quiescence and qLSC survival are *MIR300*-driven *TUG1*-regulated effects. Thus, hypoxia-induced TGFβ1-FoxM1-mediated signals increase *TUG1* expression to allow CD34⁺ CML LSC entry into quiescence and qLSC survival by maintaining the amount of free functional *MIR300* at levels sufficient for arresting cell cycle, but not for triggering PP2A-dependent apoptosis (Fig. 6A; Supplementary Fig. S6C). Conversely, *CpG-anti-miR-300* did not counteract *TUG1-shRNA*-induced apoptosis in CD34⁺ CML progenitors (Fig. 6E). Moreover, the nearly complete killing of CD34⁺ CML dividing progenitors induced by *CpG-miR-300* and *-TUG1-shRNA* combined treatment (Fig. 6E) suggests that the BCR-ABL1-regulated low *TUG1* expression in CD34⁺ CML blasts (Fig. 6B) is required for inhibiting the activity of other miRNAs negatively regulating cell survival.

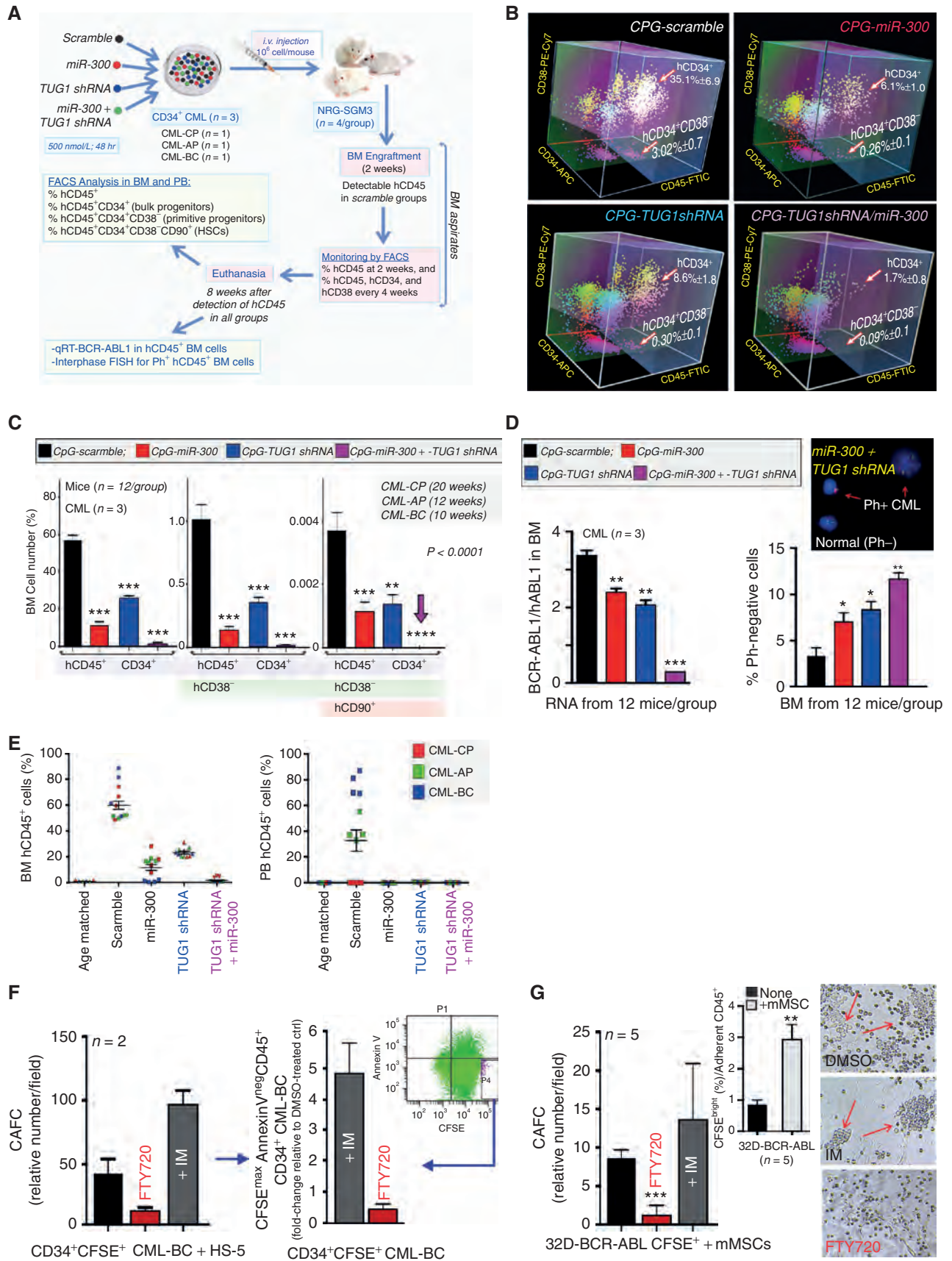
Disruption of *MIR300-TUG1* Interplay and PAD Treatment Abrogate the BMM-Protective Effect on Survival of CML qLSCs and BCR-ABL1⁺ Leukemia-Initiating Cells

By using a previously described patient-derived xenograft (PDX)-based approach suitable for determining changes in CML LT-HSC survival (40), we assessed the effects of disrupting the *MIR300-TUG1* interplay on BM-repopulating CML qLSCs. NRG-SGM3 mice ($n = 4$ /group) were transplanted with >95% Ph⁺ CD34⁺ CML-CP, -AP (accelerated phase) and -BC cells previously exposed for 48 hours to 500 nmol/L *CpG-scramble* (control), *CpG-miR-300*, and *CpG-TUG1-shRNA* used

as single agents or in combination (Fig. 7A). At 4 and 8 weeks after engraftment, BM hCD45⁺CD34⁺ progenitors and LSC-enriched hCD45⁺CD34⁺CD38⁻ cells were reduced by 75% to 97% in all arms (Fig. 7B and C). Inhibition and/or saturation of *TUG1* *MIR300*-sponging activity with *CpG-TUG1-shRNA* and *CpG-miR-300* resulted in the killing of approximately 100% of leukemia-initiating (hCD45⁺CD34⁺CD38⁻CD90⁺) quiescent HSCs (Fig. 7C), barely detectable *BCR-ABL1* transcripts, and 3.6-fold increased numbers of normal (Ph⁻) BM cells (Fig. 7D), and strongly reduced numbers of PB and BM CML (CP, AP and BC) hCD45⁺ cells (Fig. 7E). Thus, *CpG*-oligonucleotide-mediated pharmacologic disruption of *MIR300-TUG1* balance allows PP2A-mediated *MIR300* proapoptotic activity to suppress chronic and blastic CML development by selectively and efficiently eliminating nearly all TKI-resistant leukemic, but not normal quiescent HSCs and progenitors. Note that the extremely low numbers (0%–0.0015% of total BM cells recovered/12 mice/arm) of *CpG-miR-300*-, *CpG-TUG1-shRNA*-, and *CpG-miR-300/TUG1-shRNA*-treated CD34⁺CD38⁻CD90⁺ CML (CP, AP, and BC) BM-repopulating cells (Fig. 7C) did not justify serial BM transplantation into secondary and tertiary recipients.

Consistent with the role of *MIR300* as a BMM-induced tumor suppressor capable of triggering CML CD34⁺ qLSC apoptosis through suppression of SET-mediated PP2A inhibition, and with the notion that SET expression is increased in CD34⁺CD38⁻CD90⁺ CML LSCs (9) and that SET-sequestering PADs selectively induce apoptosis of TKI-resistant serially transplantable leukemic LT-HSCs and CD34⁺CFSE^{max} quiescent CML, but not normal HSCs (9), PAD treatment (2 μmol/L FTY720) of HS-5-cocultured CFSE⁺CD34⁺ CML-BC cells markedly reduced the cobblestone area-forming cell (CAFC) activity (Fig. 7F, left) and numbers of adherent CFSE^{max}AnnexinV^{neg}CD34⁺ CML qLSCs (~91.1% inhibition relative to DMSO-treated controls; Fig. 7F, right), suggesting that FTY720-mediated PP2A activation (20) circumvents the MSC-mediated protective effect on CML qLSC survival. Likewise, HS-5 CM did not protect LAMA-84 CML progenitors from FTY720-induced apoptosis (Supplementary Fig. S4D, middle). As expected (41), TKI treatment (imatinib) did not reduce, but augmented CAFC and qLSC numbers (Fig. 7F). Accordingly, FTY720, but not imatinib, strongly decreased CAFC activity (red arrows) derived from Lin⁻Sca⁺CD45⁻CD31⁺CD51⁺ mouse MSC (mMSC)-induced (inset) CFSE^{bright} 32D-BCR-ABL cells (Fig. 7G), further indicating that pharmacologic PP2A activation by SET-sequestering PADs can lead to CML eradication at qLSC level.

Figure 7. Disruption of *MIR300-TUG1* interplay and PAD treatment abrogate the BMM-protective effect on survival of CML qLSCs and BCR-ABL1⁺ leukemia-initiating cells. **A**, Xenotransplantation protocol of ex vivo-treated CD34⁺ chronic (CP), accelerated (AP) and blastic phase (BC) CML cells in NRG-SGM3 mice ($n = 4$ mice/treatment/patient sample). **B** and **C**, Analysis of *CpG-MIR300*-, *CpG-TUG1-shRNA*-, *CpG-TUG1-shRNA+CpG-MIR300*-, and *CpG-scramble*-treated CML cells from BM aspirates at 2–12 (3D plots) and 10 to 20 weeks posttransplant quantitative analysis of CML cells stained with the indicated antibodies. **D**, Evaluation at 10 to 20 weeks posttransplant of BCR-ABL1 transcripts by qRT-PCR (left) and of % Ph-negative (Ph⁻) cells by FISH (right) in total and FACS-sorted hCD45⁺BM cells, respectively. **E**, Analyses of BM CML cells at 10 to 20 weeks posttransplant: hCD45⁺ cells (%) in BM (left) and PB (right) of mice transplanted with CML (CP, AP, and BC) and treated with the indicated *CpG*-ODNs. Age-matched mice served as controls. Error bars, mean ± SEM. **F**, Effect of 2.5 μmol/L FTY720 or 1 μmol/L imatinib (IM) on CAFC activity (left) and numbers of CFSE^{max}AnnexinV^{neg}hCD45⁺CD34⁺ CML qLSCs derived from CFSE-labeled CD34⁺ CML-BC cells cocultured for 7 days on BM-derived HS-5 MSC cells (right). Inset, FACS plot shows gating of CFSE^{max} CML qLSCs. **G**, Relative number and representative images of CAFC (red arrows) of CFSE-labeled 32D-BCR-ABL cells cocultured with primary mMSCs in the absence or presence of IM (1 μmol/L, 48 hours) or FTY720 (2 μmol/L, 48 hours; $n = 5$). Inset: CFSE^{bright} fraction of adherent 32D-BCR-ABL cells in medium and cocultured for 4 days with mMSCs. Range values of controls are reported in Supplementary Table S1.



DISCUSSION

Altered miRNA expression and PP2A tumor suppressor activity are tightly linked to leukemogenesis and impaired NK-cell-mediated anticancer immunity. The notion that PADs, but not TKIs, kill CML qLSCs (42) implies that BCR-ABL1 kinase-independent signals, likely arising from the endosteal hypoxic BMM (5), regulate CML LSC activity and survival through inhibition of PP2A. We previously reported that BCR-ABL1 expression, but not activity, is essential for recruitment of Jak2-driven hnRNPA1-mediated signals inducing SET-dependent PP2A inhibition that, in turn, allows CTNNB1 (β -catenin)-dependent regulation of CML (CP and BC) LSC proliferation and survival (9). We also demonstrated that inhibition of cytokine-induced SET upregulation or PAD treatment impair NK-cell cytotoxicity against Ph⁺ cells through activation of PP2A (30). Here we showed that post-transcriptional signals, which are initiated by the tumor-naïve BMM and likely maintained by the tumor-resaped BMM, control CML LSC entry/maintenance into quiescence and impair NK-cell immunity. This occurs through the induction of *MIR300*, a tumor suppressor miRNA with dose-dependent antiproliferative and PP2A-activating functions, which are uncoupled and differentially regulated by *TUG1* lncRNA decoy activity in CML LSCs. Importantly, a dose-dependent target selection mechanism (43) allows the sequential activation of *MIR300* antiproliferative and PP2A-activating functions through the inhibition of CDK6/CCND2 and SET, respectively, in CML qLSCs and progenitors and in NK cells.

MIR300 Role in CML LSCs and Progenitors

Expression studies revealed that *MIR300* levels are downregulated in CML (CP and BC) CD34⁺ progenitors, but not in the CML-initiating (1) qLSC (CD34⁺CFSE^{max}) fraction. Restoration of *MIR300* expression arrested proliferation, expanded the G₀-G₁ quiescent stem cell fraction, strongly impaired survival of dividing CD34⁺ CML stem/progenitor cells, and was associated with downregulation of CCND2/CDK6, SET, and other PP2A-regulated CML growth- and survival-promoting factors (e.g., JAK2, CTNNB1, hnRNPA1 and MYC; ref. 1). Because CCND2/CDK6 inhibition characterizes quiescent long-term HSCs (LT-HSCs) and is sufficient to arrest CD34⁺ leukemic progenitors in G₀-G₁ (21, 22), *MIR300*-induced loss of CCND2/CDK6, which occurs at low levels of *MIR300* expression, likely represents the mechanism by which *MIR300* antiproliferative activity contributes to CML stemness. Likewise, SET inhibition, which occurs when *MIR300* is highly expressed and is sufficient for triggering PP2A-mediated cell death of CML (CP and BC) qLSC and progenitors (8, 9), likely account for *MIR300*-induced apoptosis. In fact, we showed that loss of *MIR300* binding to SET impaired *MIR300*-induced PP2A-mediated Ph⁺ cell apoptosis. This also suggests that inactivation and/or downregulation of JAK2, CTNNB1, Twist1, and MYC may result from *MIR300*-induced PP2A activation. Indeed, bioinformatics analysis that integrates several algorithms and also takes into account miRNA and mRNA targets' expression levels in normal and myeloid leukemia BM cells indicated that *MIR300*-induced inhibition of other PP2A-regulated survival factors (e.g., Twist1, CTNNB1, JAK2, and MYC) requires

levels of *MIR300* significantly higher than those suppressing SET (Fig. 2B; Supplementary Fig. S3B). Thus, downregulation of these *MIR300* targets unlikely represent the primary mechanism of *MIR300*-induced apoptosis of CML qLSCs and progenitors. Strengthening the importance of CCND2/CDK6 and SET as key *MIR300* effectors is the notion that *MIR300*-induced CCND2/CDK6 and SET inhibition may not be limited to *MIR300*-induced posttranscriptional downregulation. In fact, *MIR300* may also impair SET, CCND2 and/or CDK6 transcription, mRNA nuclear export, translation and/or protein stability/activation upon inhibition of other PIP factors (e.g., hnRNPA1, JAK2, and SETBP1), and the associated XPO1 (Supplementary Fig. S3A, left; refs. 8, 20, 44–46).

The evidence that high levels of *MIR300* expression does not induce apoptosis of CML qLSCs, which exhibit inactivation of PP2A and activation of JAK2, SET, and CTNNB1 (1, 9), raises the questions of whether *MIR300* is required for LSC quiescence and survival; how *MIR300* is regulated in qLSCs and leukemic progenitors; and how qLSCs elude *MIR300*-induced apoptosis.

The requirement of *MIR300* for induction and maintenance of CML LSC quiescence is clearly demonstrated (Figs. 2D, 3B, and 4C; Supplementary Fig. S4D) by: (i) the ability of anti-*MIR300* molecules to antagonize MSC-induced inhibition of leukemic cell proliferation, (ii) impaired LTC-IC-driven colony formation in the absence of qLSC apoptosis in CD34⁺ cells exposed to CpG-miR-300 concentrations inhibiting CCND2/CDK6 but not SET expression, and by the (iii) inability of MSCs to induce SET downregulation in CML cells. Importantly, the evidence that *MIR300*-dependent SET inhibition is induced by hypoxia, but not MSCs, in CD34⁺ CML stem/progenitor cells (Fig. 4A; Supplementary Fig. S4D) and that SET, JAK2, and CTNNB1 are active in CML qLSCs (1, 46), suggests that LSC entrance into quiescence is initiated by MSCs prior to LSC niching into the BM endosteal area with the lowest O₂ tension in which the *MIR300* PP2A-activating proapoptotic function is likely inhibited by the hypoxia-induced *TUG1* sponging activity. Moreover, the evidence that anti-*MIR300*-expressing MSCs fail to suppress leukemic CD34⁺ cell proliferation, and that exposure of CD34⁺ CML stem/progenitor cells to MSC CM and/or exosomes increases *MIR300* expression and double the number of CD34⁺ CML cells in the quiescent LSC compartment (Fig. 4), suggests that the MSC-induced transition into quiescence of CD34⁺ CML LSCs/progenitors may depend on CDK6/CCND2 downregulation induced by MSC-derived exosomal *MIR300*. In this scenario, hypoxia-induced *MIR300* will sustain, but not promote, CML LSC quiescence. However, MSCs may contribute to the hypoxia-dependent regulation of *MIR300*-induced LSC quiescence and qLSC survival by increasing *TUG1* expression through the release of TGF β 1 (36). Mechanistically, we showed that hypoxia induces *MIR300* transcription in CD34⁺ CML cells and MSCs through reduced LIP (inhibitory) and increased LAP1 (activatory) C/EBP β , which binds/transactivates a hypoxia-sensitive regulatory element located 109 bp upstream the *MIR300* gene. Accordingly, it was found that C/EBP β was found expressed in CML LSCs (26), induced by hypoxia, and to negatively regulate G₁-S transition and SET expression (47, 48).

Although other miRNAs regulating LSC survival or qLSC reentry into cycle have been associated with CML development (18, 49, 50), to our knowledge, *MIR300* is the only cell

context-independent (same activity in LSCs and progenitors) miRNA capable of both supporting CML leukemogenesis by inducing LSC quiescence and triggering CML qLSC and progenitor cell apoptosis.

MIR300 Role in NK Cells

MIR300 is also the only tumor-naïve-induced tumor suppressor miRNA that inhibits NK cell-mediated innate anticancer immunity while promoting LSC quiescence. NK cells preferentially kill cancer stem cells (4, 51), including BM-repopulating TKI-resistant BCR-ABL1⁺ qLSCs (Fig. 5B), and NK-cell quantitative and functional impairment is a feature of patients with untreated and TKI-treated CML (6, 52). Impaired NK-cell immunity also associates with CML qLSC persistence in patients with TKI-treated CML in deep molecular remission (28, 31), whereas normal levels of activated NK cells characterize patients in sustained treatment-free remission (28) and account for increased disease-free survival after T-cell-depleted stem cell transplant (4), suggesting that NK-cell-based therapies may lead to qLSC eradication.

Despite RNA sequencing (RNAseq) of MSC exosomal RNA suggesting that other 14 MSC-derived miRNAs may contribute to impaired NK-cell activity (Supplementary Fig. S5C), we showed that *MIR300* levels are increased in circulating NK cells from patients with CML at diagnosis and that BMM-induced inhibition of NK cell proliferation and antitumor activity require *MIR300* induction. In fact, BMM-induced NK cell inhibition was recapitulated by *MIR300* mimics and abrogated by *MIR300* RNAi. Furthermore, our data suggests that impaired NK-cell proliferation and cytotoxicity may depend on C/EBPβ-*MIR300* signals leading to CCND2/CDK6 and SET downregulation. Because the tumor-naïve BMM-induced loss of CCND2 and SET expression (PP2A inhibition) account for suppression of NK cell proliferation (29) and antitumor cytotoxicity (30), the NK cell quantitative and qualitative defects observed in CML may arise from *MIR300*-mediated signals initiated by the naïve BMM (53), sustained and/or exacerbated by the leukemia-reshaped BMM (54) and overriding cytokine-driven NK cell activation (55). Interestingly, treatment with MSC exosomes also reduced pre-miR-155 levels (BIC) in IL12/IL18-stimulated and resting NK-92 cells (Supplementary Fig. S5D). Because, miR-155 not only inhibits SHIP1 and PP2A to allow MAPK- and AKT-dependent NK cell proliferation and cytotoxic activity (16, 55), but also suppresses C/EBPβ expression (ref. 56; Supplementary Fig. S5D), MSC-induced BIC downregulation likely contributes to *MIR300*-dependent NK cell inhibition by antagonizing miR155-induced C/EBPβ downregulation. Furthermore, consistent with the notion that *TUG1* acts as a *MIR300* decoy and in contrast with the mechanism regulating *MIR300* activities in leukemic cells, BMM-induced NK cell inhibition occurs in a *MIR300*-dependent, but not *TUG1*-independent manner; in fact, hypoxia did not increase, but decreased *TUG1* expression in NK cells, and *TUG1*-shRNAs did not alter NK cell number (Supplementary Fig. S5E and S5F).

Biological and Therapeutic Relevance of the MIR300-TUG1 Interplay in CML Cells

TUG1 is an oncogenic lncRNA upregulated in different types of cancer in which it has strong diagnostic, prognostic

and therapeutic relevance (34). In CML-BC qLSCs, *TUG1* is induced by hypoxia and uncouples *MIR300* functions and dose-dependently suppresses only *MIR300* PP2A-mediated proapoptotic activity (Fig. 6). This unprecedented lncRNA function allows *TUG1* to maintain unbound *MIR300* at levels sufficient for inducing CML LSC growth arrest but not for triggering PP2A-mediated apoptosis, which does not depend on loss of *TUG1* survival signals, but on the effect of freed *MIR300* on SET mRNA. Accordingly, *TUG1* loss in solid tumors was associated with G₀-G₁ arrest and apoptosis, whereas its overexpression with induction of proliferation and upregulation of mitogenic and survival factors (e.g., CCND1/2, CTNNB1, and Twist1) also described as *MIR300* targets (34). In addition, we showed that *TUG1* activity is *MIR300*-restricted in CD34⁺ CML qLSCs, but not in leukemic progenitors in which *TUG1*-shRNAs induced apoptosis of anti-*MIR300*-treated CD34⁺ CML cells. Because *TUG1* interacts with several tumor suppressor miRNAs (34, 57), this suggests that *TUG1* may function in CML LSCs and progenitors as a hub for specific subsets of functionally related tumor suppressor miRNAs. Indeed, 56 experimentally validated *TUG1*-interacting miRNAs that possess growth-suppressive and/or proapoptotic functions are differentially expressed in CD34⁺CD38⁻ LSC-enriched and CD34⁺CD38⁺-committed progenitor CML (CP and BC) cells (Supplementary Fig. S7A). Notably, 96.4% and 44.3% of these miRNAs are predicted to shut down BCR-ABL1-dependent signals in CML blasts and, like *MIR300*, to act as inhibitors of cell-cycle progression and PP2A activators (Supplementary Fig. S7A and S7B). Thus, it is conceivable that balanced *TUG1*-*MIR300* levels are essential for CML qLSC induction/maintenance, whereas insufficient *TUG1* expression will lead to CML qLSC and progenitor cell apoptosis by freeing *MIR300* and other miRNAs with similar tumor suppressor activities. Conversely, high *TUG1* sponge activity will likely promote CML cell proliferation, survival, and qLSC cell-cycle reentry, although an aberrant *TUG1* increase that also inhibits *MIR300* antiproliferative activity may induce LSC exhaustion by impairing entry into quiescence and forcing reentry into cycle.

Mechanistically, we showed that increased *TUG1* expression in qLSCs depends on hypoxia-induced TGFβ1 secretion by CD34⁺ CML stem/progenitor cells. In fact, exposure to a TGFβ1 blocking antibody markedly impaired *TUG1* expression in CML progenitors and in hypoxia-cultured CML qLSCs. However, hypoxia-induced TGFβ1/2 upregulation in CML LSCs (36) may also contribute to increased *TUG1* expression and regulation of *MIR300* functions. Hypoxia-induced *TUG1* expression in CML qLSCs may also depend on Notch activity (58); however, blocking TGFβ1 signaling in CD34⁺ CML progenitors and hypoxia-exposed qLSCs also strongly suppressed expression of FoxM1, a *TUG1* transcriptional inducer and regulator of CML LSC quiescence and cycling activity (37, 39, 50). Thus, hypoxia-TGFβ-FoxM1, but not Notch-induced signals, increases *TUG1* expression in CML LSCs to selectively inhibit *MIR300* PP2A-mediated proapoptotic function while allowing *MIR300*-dependent entry into quiescence. However, Notch signaling may contribute to the *MIR300*-*TUG1*-dependent regulation of LSC quiescence and survival through the RBPJ-mediated inhibition of miR-155 that may induce *TUG1* and *MIR300* expression by

preventing FoxM1 and C/EBP β downregulation, respectively (Supplementary Fig. S6C).

In conclusion, tumor-naïve BMM-induced *MIR300* tumor suppressor antiproliferative and PP2A-activating functions support CML development through induction of LSC quiescence and inhibition of NK cell-mediated qLSC killing, respectively. This may represent the initial step leading to formation and expansion of the TKI-resistant CML qLSC pool. Once established, the CML clone will reshape the BMM to further support disease development and progression. *TUG1-MIR300* interaction plays a central role in this process because altering its ratio leads to the nearly complete and selective PP2A-dependent eradication of chronic and blastic CML qLSCs *in vitro* and in PDXs. This, together with the ability of SET-sequestering PADs to bypass the MSC-induced protective effect on CML qLSC survival, not only highlights the therapeutic importance of pharmacologically modulating PP2A activity in anti-LSC and NK cell-based therapeutic approaches for CML eradication, but also indicates that the activity of a tumor suppressor (i.e., *MIR300*) can be exploited by LSCs to preserve their ability to induce and maintain leukemia.

METHODS

Cell Culture and Treatments

Cell Lines Ph⁺ CML-BC K562 and LAMA-84, human BM MSC-derived HS-5 (59), mouse BM-derived 32D-BCR/ABL, and the clinically relevant human NK-92 (60) cells were cultured in RPMI1640 medium. NK-92 cultures were supplemented with 150 IU/mL rhIL2 (Hoffmann-La Roche, Inc.). The amphotropic-packaging 293T and Phoenix cells were cultured in DMEM. All tissue culture media were supplemented with 10% to 20% heat-inactivated FBS (Gemini; Invitrogen), 2 mmol/L L-glutamine, and 100 U/mL penicillin/streptomycin (Invitrogen). Cell lines were obtained from ATCC, authenticated by FACS, qRT-PCR, or immunoblotting phenotypical analyses and used at low passages and tested for *Mycoplasma* contamination using a MycoAlert Mycoplasma Detection Kit (Lonza, Inc.).

Primary Cells Human hematopoietic stem and progenitor cell fractions from healthy and leukemic individuals were isolated from BM, PB, or UCB. Prior to their use, cells were kept (18 hours) in StemSpan CC100 cytokine-supplemented SFMII serum-free medium (Stemcell Technologies). Human BM MSCs (hMSCs) from healthy individuals were isolated from BM cells by Ficoll-Hypaque density-gradient centrifugation followed by culture in complete human MesenCult Proliferation Kit medium and used for CM and exosome purification (Supplementary Methods). Human CD56⁺CD3⁻ NK cells (purity >95%) from healthy (UCB or PB), CML (CP, BC and AP) individuals were FACS and/or magnetic (Miltenyi Biotec, Inc.) cell sorted, or RosetteSep Ab-purified (Stemcell Technologies) as described previously (30).

Frozen CML leukemia specimens were from the Leukemia Tissue Banks located at The University of Maryland (UMB, Baltimore, MD), The Ohio State University (Columbus, OH), Maisonneuve-Rosemont Hospital Research Centre, Montreal (Quebec, Canada), Hammersmith Hospital, Imperial College (London, United Kingdom), "Policlinico-Vittorio Emanuele" (Catania, Italy), University of Utah (Salt Lake City, UT), Hematology Institute Charles University (Prague, Czech Republic), and Aarhus University Hospital (Aarhus, Denmark); fresh UCB, NBM, and PB (CML and healthy individuals) samples were purchased (Lonza, Inc.) or obtained from UMB Hospital (Baltimore, MD) and Maisonneuve-Rosemont Hospital Research

Centre, Montreal. Patient samples were not collected for this study, which was carried out with a waiver of informed consent and approval from the University of Maryland Institutional Review Board (IRB). UCB units were collected at the University of Maryland Medical Center with IRB-approved protocol and written informed consent.

mMSCs were isolated as described previously (61). Briefly, BM was flushed from femurs and tibias of FVB/N mice. Bones were fragmented to small chips (1–2 mm) and digested with 1 mg/mL collagenase for 2 hours at 37°C. Digested bones were grown in mouse MesenCult MSC Basal Medium supplemented with Mesenpure and MSC Stimulatory Supplement (Stemcell Technologies). Purity (Lin⁻CD45⁻CD31⁻CD51⁺Sca1⁺>90%) of isolated cells was confirmed by flow cytometry using anti-Lin Pacific Blue, CD45 PE-Cy7, CD31 FITC (BioLegend), CD51 PE, and Sca1 APC (eBioscience) antibodies. Cells were kept for a maximum of five passages. mMSC CM was obtained by culturing 50% to 70% confluent mMSCs in IMDM supplemented with 10% FBS and 2 mmol/L L-glutamine for 48 hours.

Cells were treated for the indicated time and schedule with 1–2 μ mol/L imatinib mesylate (IM; Novartis), 5 μ mol/L 5-Aza-2'-deoxycytidine (5-Aza; Sigma), 250–500 nmol/L *CpG-scramble*, *-miR-300*, *-anti-miR-300*, and *-TUG1-shRNA* oligonucleotides (ODN; Beckman Research Institute, City of Hope, Duarte, CA), 1.25 μ g/mL anti-TGF β neutralizing antibody (1D11; R&D Systems), 10 ng/mL rhIL12 and 100 ng/mL rhIL18 (R&D Systems), and 2 μ mol/L FTY720 (Fingolimod, Sigma). Where indicated, cells were cultured for the indicated times in hypoxic conditions (1% O₂), HS-5 and hMSC CM (100% vol/vol), or in medium supplemented with MSC-derived exosomes (50–100 μ g/mL). During treatments, viable cells were enumerated by the trypan blue exclusion test.

Flow Cytometry and Cell Sorting

CD34⁺, CD34⁺CD38⁻, CD34⁺CD38⁺ fractions were magnetic (CD34 MicroBead Kit; Miltenyi Biotec) and/or FACS (α CD34 APC/PE and α CD38 PE/Cy7 Abs, BD Biosciences) purified (purity: >90%–100%). Primary human NK cells were sorted using Alexa Fluor 488 α hCD56, PE-Cy5 α hCD19c and PE-Cy7 α hCD3 Abs (BD Biosciences) and their purity assessed by PE α CD56 (Beckman Coulter, Life Sciences) and APC-eFluor780 α CD3 (eBioscience) antibody staining. hMSC purity (>99%) was assessed by flow cytometry using anti-CD34 and CD45 FITC, CD73 PE-Cy7, CD105 Alexa 647, CD44 Percp-Cy5.5, and CD90 PE antibodies (BD Biosciences). Apoptosis was quantified by FACS upon staining cells with PE Annexin-V and 7-ADD (BD Biosciences). Cells were sorted using the FACS Aria II (BD Biosciences). Data acquisition and analyses were performed at the UMBCCC Flow Cytometry Facility. Data from LSRII or CANTO II flow cytometers (BD Biosciences) were analyzed by using either the FlowJo v8.8.7 or Diva v6.1.2 software.

LTC-IC and CFC/Replating Assays

CD34⁺ CML (CP and BC) and UCB cells were lentivirally transduced/GFP-sorted and/or treated (500 nmol/L, 3 days) with *CpG-ODN* to ectopically express either *MIR300* or anti-*MIR300* RNAs prior to use in LTC-IC and CFC assays (46). Vector-transduced and CpG-scramble-treated cells served as controls.

LTC-ICs A total of 2×10^5 CML and 2×10^3 UCB CD34⁺ cells were cultured with a 1:1 mixture of irradiated (80 Gy) IL3/G-CSF-producing M2-10B4 and IL3/KL-producing SI/SI murine fibroblasts in MyeloCult H5100 (Stemcell Technologies) supplemented with hydrocortisone. Medium was replaced after 7 days, followed by weekly half-medium changes, and fresh 500 nmol/L *CpG-ODN* where required. After 6 weeks, adherent and floating cells were harvested, and 5×10^3 CML and 2×10^3 for UCB cells were plated into cytokine (KL, G-CSF, GM-CSF, IL3, and IL6) supplemented MethoCult H4435. LTC-IC-derived colonies were scored after 14 days.

CFCs and CFC/replating Assays CD34⁺ and CD34⁺ CD38⁻ CML (5×10^3) and/or UCB (2×10^3) cells were seeded in MethoCult H4435 supplemented with Epo, KL, G-CSF, GM-CSF, IL3, and IL6. Fourteen-day colonies were mixed and the same number of cells replated twice (first and second replating) and scored 2 weeks later.

CFSE (or eFluor670)-Mediated Tracking of Cell Division

CFSE (CellTrace CFSE Proliferation Kit, Invitrogen) or eFluor670 (Cell Proliferation Dye eFluor670; eBioscience)-stained cells were FACS sorted to isolate the highest fluorescent peak, treated as indicated, harvested after 4 to 5 days, and counterstained with Near-IR Fluorescent Dye (Live/Dead Cell Stain Kit, Invitrogen) to determine the number of viable dividing (CFSE/NearIR⁻) and quiescent cells (CFSE^{max}/NearIR⁻). Where indicated, cells were stained with anti-CD34 APC and sorted into dividing and quiescent subpopulations. Quiescent stem (CFSE^{max}CD34⁺) and dividing progenitor cells in each peak were reported as a fraction of the initial number of CD34⁺ cells (46). For NK cells, 4- and 7-day-cultured CFSE-labeled NK-92 and primary NK cells, respectively, were α CD56 APC Ab- and Aqua Fluorescent Dye (Live/Dead Cell Stain Kit, Invitrogen) stained. NK cells were used in cytotoxicity assays and proliferation was quantitated as fold changes of CFSE mean fluorescence intensity in living CD56⁺ NK cells.

Plasmids

pCDH-miR-300 (hsa-miR-300) pCDH-MIR300 was generated by subcloning a 490 bp *NheI*-*Bam*HI PCR fragment encompassing the mature hsa-MIR300 into the pCDH-CMV-MCS-EF1-copGFP-puro (SBI) vector. Sequence was confirmed by sequencing.

pSIH-H1-Zip-MIR300 (pZip-MIR300) To knockdown *MIR300*, a 5'-*Eco*RI and 3'-*Bam*HI-flanked *MIR300* antisense dsODN was directionally cloned into the pSIH1-H1-copGFP vector (SBI).

pSIH-H1-copGFP-shTUG1 (TUG1 shRNA) A shRNA cassette containing the targeted nt 4571 to 4589 of *hTUG1* RNA (58) was subcloned into pSIH-H1-copGFP vector (SBI). A nonfunctional scrambled *TUG1* shRNA was used as a control.

pLenti-TUG1 The *hTUG1* into the pLenti-GIII-CMV-GFP-2A-Puro-based vector was from Applied Biological Materials, Inc.

pGFP/Luc-based MIR300 Promoter Constructs p513-GFP/Luc, p245-GFP/Luc, and p109-GFP/Luc were generated by cloning the -522 bp, -245 bp, and -109 bp regions upstream the hsa-MIR300 gene locus (Sequence ID: NC_000014.9) into pGreenFire1 (pGFP/Luc, pGF1; SBI) reporter vector. The regions upstream the hsa-MIR300 gene were PCR amplified from K562 DNA and cloned into the pGF1 *Eco*RI-blunted site.

p109-C/EBP β mut-GFP/Luc An *Eco*RI-containing double-stranded synthetic oligonucleotide spanning the -109 bp *MIR300* regulatory region and containing the T/G and C/G mutated C/EBP β consensus binding sites located at positions -64 and -46, respectively, was subcloned into *Eco*RI-digested pGF1 vector. pCDH-Flag-SET, fluorescent ubiquitination-based cell-cycle indicator reporter pCDH-FUCCI2BL, MigR1- Δ uORF-C/EBP β -ER^{TAM}, and MigR1- Δ uORF-C/EBP α -HA constructs were described previously (25, 62–64).

pCDH-Flag-SET 3'UTRwt-GFP and pCDH-Flag-SET Δ 3'UTR-GFP Wild-type (627 bp) or 3'-deleted (513 bp) SET 3'UTRs were PCR amplified from K562 cDNA using a common *Eco*RI-linked 5'-primer and specific *Bam*HI-linked 3'-primers for the wild-type and deleted

SET mRNA 3'UTR. The PCR products were cloned into the pCDH-Flag-SET plasmid and sequenced.

MSC CM and Exosome Purification

HS-5- and hMSC-derived CM was obtained by culturing cells in complete RPMI (24 hours) and StemSpan SFMII (48 hours) medium, respectively. Alix⁺CD63⁺ exosomes were purified by differential centrifugation ($3,000 \times g$, 15 minutes; $10,000 \times g$, 10 minutes; and $100,000 \times g$, 70 minutes) from HS-5 CM cultured in exosome-free FBS-supplemented medium (65, 66). When required, exosomes were precipitated (Exo-Quick; SBI) prior to isolation by ultracentrifugation.

Lentiviral and Retroviral Transduction

Lentiviral or retroviral particles were produced by transient calcium phosphate transfection (ProFection Mammalian Transfection System, Promega) of 293T and Phoenix cells, respectively (8, 9, 67). Briefly, viral supernatant was collected 24 and 48 hours after transfection and directly used or concentrated by PEG precipitation. Viral titer was determined by flow cytometry by calculating number of GFP⁺ 293T cells exposed (48 hours) to different viral dilutions. One to three spinoculation rounds were used for cell line infection, whereas a single spinoculation with diluted viral supernatants (MOI = 6) was used for primary cells. Viral supernatants were supplemented with polybrene (4 μ g/mL). FACS sorting or puromycin selection was initiated 48 hours after transduction.

Cell-cycle Analysis

Cell-cycle analysis was performed by 4',6'-diamidino-2-phenylindole (DAPI)/Ki-67 staining of *CpG-scramble*- or *CpG-miR-300*-treated (500 nmol/L; 72 hours) primary CD34⁺ CML (CP and BC) and UBC cells as described previously (64). Briefly, cells were fixed, permeabilized (Cytofix/Cytoperm kit, BD Biosciences), and Ki-67 PE (BioLegend) and DAPI (Sigma) stained. Alternatively, cell-cycle analysis was performed on pCDH-Fucci2BL-infected cells and subjected to flow cytometric analysis. LAMA-84-FUCCI2BL⁺ CML-BC cells were exposed to 500 nmol/L *CpG-scramble* and *CpG-miR-300* oligonucleotides after being G₁-S synchronized (4–6 μ mol/L aphidicolin, 6 hours). *CpG-oligo*-treated (48 hours) FUCCI2BL⁺ cells were subjected to live-cell imaging for 48 hours and analyzed as described previously (64). Briefly, *CpG-scramble*- or *CpG-miR-300*-treated cells in G₀-G₁ were mVenus⁻ PE-Texas-Red⁺, G₁-S cells were mVenus⁺ PE-Texas-Red⁺, and S-G₂-M cells were mVenus⁺ PE-Texas-Red⁻.

Live-Cell Imaging and Confocal Microscopy

Wide-field fluorescence imaging of *CpG-ODN*-treated pCDH-FUCCI2BL-transduced LAMA-84 cells was executed with an Olympus Vivaview digital camera, maintained at humidified atmosphere 37°C with 5% CO₂, mounted into a microscope-equipped incubator with green and red fluorescence filters. Emission spectral ranges were green-narrow (490–540 nm) and red-narrow (570–620 nm). Imaging was carried out for 24 or 48 hours. Confocal fluorescence images were acquired using a LEISS LSM510-inverted confocal microscope equipped with 40 \times /1.2-NA water immersion objective with 0.55- μ m pixel size. Cell-cycle phases were determined by plotting average red and green fluorescent intensity over time using Prism 6.0 d software. The Vivaview raw images were reconstructed using ImageJ v5.2.5 and Adobe CS6 software.

Real-time RT-PCR

Total RNA was extracted using miRNeasy Micro Kit (Qiagen Inc.) or TRIzol (Invitrogen) and reverse transcribed using a standard cDNA synthesis or the TaqMan MicroRNA Reverse Transcription Kit

with mouse and/or human-specific sets of primers/probe for *BCR-ABL1*, *CEBPB*, *FOXM1*, *TUG1*, *IFN γ* , *pri-MIR300*, *MIR300*, *pre-miR-155* (*BIC*), *18S*, *RNU44*, *RNU6B*, and *snoRNA202* (Applied Biosystems). PCR reactions were performed using a StepOnePlus Real Time PCR System (Applied Biosystems). Data were analyzed according to the comparative C_t method using *RNU44*, *RNU6B*, *18S*, and *snoRNA202* transcripts as an internal control. Results are expressed as fold change of mean \pm SEM.

Immunoblot Analysis

Lysate from cell lines and primary cells were subjected to SDS-PAGE and Western blotting as described previously (46). The antibodies used were anti-actin, anti-Myc, anti-C/EBP β , anti-Alix, anti-Twist, and anti-CD63 (Santa Cruz Biotechnology); anti-GRB2 (Transduction Laboratories); anti-JAK2, anti- β -catenin, anti-FoxM1, anti-CDK6, anti-pJAK2^{Y1007/1008}, and anti-CCND2 (Cell Signaling Technology); anti-SET (Globozymes); anti-ABL (Ab-3), anti-CCND1/2, anti-PY (4G10), and anti-PP2Ac^{Y307} (EMD); anti-hnRNPA1 (Abcam); and anti-Flag (M2; Sigma).

PP2A Phosphatase Assay

PP2A assays were performed using the malachite green-based PP2A Immunoprecipitation Phosphatase Assay Kit (Millipore) as described previously (46). Briefly, protein lysates (50 μ g) in 100 μ L of 20 mmol/L HEPES pH 7.0/100 mmol/L NaCl, 5 μ g α PP2Ac Ab (Millipore), and 25 μ L protein A-agarose was added to 400 μ L of 50 mmol/L Tris pH 7.0, 100 mmol/L CaCl₂. Immunoprecipitates were carried out at 4°C for 2 hours and used in the phosphatase reaction according to the manufacturer's protocol.

Luciferase Assay

Transcriptional activity of the intergenic 513 bp region upstream the *MIR300* gene was investigated by Luciferase assay using the pGreenFire-Lenti-Reporter system (pGF1; SBI) in cell lines and primary CD34⁺ CML-BC cells. Briefly, cells were transfected with constructs containing wild-type full-length 513 (p513-GFP/Luc) and deleted 245 (p245-GFP/Luc) and 109 (p109-GFP/Luc) base pair-long region upstream the *MIR300* gene locus, or with the p109-GFP/Luc construct mutated in the two C/EBP β -binding sites (p109-CEBP β mut-GFP/Luc). The empty vector (pGFP-Luc; pGF1) was used as a negative control. After 48 hours, cells were lysed and luciferase activity was determined by Pierce Firefly Luciferase Flash Assay Kit (Thermo Scientific).

Cytotoxicity Assays

A flow cytometry-based killing assay was performed using K562 cells as targets (68). Briefly, HS-5-derived CM (100% vol/vol) or exosomes (50–100 μ g/mL) preconditioned (36 hours in 50–150 IU/mL IL2) NK-92 cells were cocubated (3.5 hours) with CFSE-labeled K562 cells at ratio 5:1. Killing was evaluated by assessing the percentage of Annexin-V⁺ cells on CD56⁻ and/or CFSE⁺ target cells. When CpG-ODNs were used, NK-92 cells were preconditioned (36 hours) in medium lacking IL2. NK-92 cell-killing of qLSCs was performed using CFSE-labeled CD34⁺ CML-BC cells cultured (4 days) in cytokine-supplemented StemSpan II Serum-Free Expansion Medium exposed (18 hours) to NK-92 cells. Spontaneous cytotoxicity toward qLSCs was determined by FACS-mediated evaluation of LSC numbers in Annexin V^{high}CD34⁺CFSE^{max} cells before and after exposure to NK-92 cells.

LSC Engraftment and Disease Development in NRG-SGM3 Mice

In vivo evaluation of changes in BM-repopulating LSCs was performed as described previously (40). A total of 10⁶ BM CD34⁺ CML

($n = 3$; >95% Ph⁺; CP, AP, and BC) cells, treated (500 nmol/L, 48 hours) *ex vivo* with CpG-ODNs, were intravenously injected (4 mice/treatment group/patient sample) into sublethally irradiated (2.6 Gy) 6 to 8-week-old NOD.Cg-Rag1^{tm1Mom} Il2rg^{tm1Wjl} Tg(CMV-IL3, CSF2, KITLG)1Eav/J mice (NRG-SGM3; The Jackson Laboratory). Engraftment was assessed by anti-human CD45 (BD Biosciences) flow staining of intrafemur BM aspirates (46) at 2 weeks in CpG-scramble control groups and at 2, 4, and 12 weeks posttransplant in CpG-MIR300, -TUG1shRNA, and MIR300+TUG1shRNA CML-BC, AP, and CP, respectively. Animal studies were performed according to IRB- and Institutional Animal Care and Use Committee-approved protocols.

Oligonucleotides and Primers

The partially phosphothioated (*) 2'-O-Methyl ODNs were linked using 5 units of C3 carbon chain linker, (CH₂)₃ (X). The ODNs were synthesized by the DNA/RNA Synthesis Laboratory, Beckman Research Institute of the City of Hope (Duarte, CA).

CpG-oligonucleotides and Probes

CpG-miR-300: 5'-g*g*tgcatcgatgcagg*g*g*g*gxuuuuuauacaagggcagacucucucu-3'
CpG-anti-miR-300: 5'-g*g*tgcatcgatgcagg*g*g*g*gxuuuuuagagagagucugccuuuuuu-3'
CpG-Tug1-shRNA: 5'-g*g*tgcatcgatgcagg*g*g*g*gxuuuuuacucugggcuucugcac-3'
CpG-scramble: 5'-g*g*tgcatcgatgcagg*g*g*g*gxuuuuuagaaaccguacucguacuuu-3'

pCDH-CMV-MCS-EF1-copGFP-puro miRNA Constructs

MIR300(F): 5'-gctagctgtgactagttgtacctag-3'; MIR300 (R): 5'-gatcctctcttcagaaagttcttg-3'

pSIH1-H1-copGFP Constructs

Zip-MIR300 ODN: 5'-gatatgttcccgtctgagagagagaaggacagctctctctctcagcgggaacatataaaaacttaa-3'
shTUG1(+): 5'-gatccgtgcagaagccagagtaattcaagagattactctgggcttctgacattttg-3'
shTUG1 (-): 5'-aattcaaaaagtcagaagccagagtaattcttgaattactctgggctctgacag-3'

pCDH-Flag-SET Constructs

SET3'UTRwt-GFP(F): 5'-gaattctactcttttctctctctctctgtata-3'; SET3'UTRwt-GFP(R): 5'-cggatccgtatacaagtcacaaact-3'
SETA3'UTR-GFP(F): 5'-ggatccagagaaaagcatcaca-3'; SETA3'UTR-GFP(R): 5'-cggatccgtatacaagtcacaaact-3'

pGreenFire1

p522-pGF1(F): 5'-ccggaattccggcagcttttctgactatcaaatgct-3'
p245-pGF1(F): 5'-ccggaattccgggtgaaccttttactgtgactagttg-3'
p109-pGF1(F): 5'-ccggaattccgggtgtgctgctctccacat-3'
Common(R): 5'-tgctctagagcaaatgatggcagtgacagaa-3'

p109-C/EBP β Mutant Construct

(+) strand ODN: 5'-aattc ggtgtgctgc tctccatg catgcccac ctgtgtctct aagcctggct cctggagctg gtgggaactt agtcacagag gaaatggcctctctgact gccatcttg-3'
(-) strand ODN: 5'-caatgatggc agtgacagga aggccattc ctctgtgact aagttccac cagctccagg agccagcctt agagacaca gatgggatct gcatggtgag agcagcac cgaatt-3'

Bioinformatics Tools

Statistically significant ($P < 0.05$ with FDR correction) predicted and validated hsa-miR-300 mRNA targets according to mRNA target

function and *MIR300* doses were identified using DIANAmicroT-CDS (diana.imis.athena-innovation.gr), ComiR (<http://www.benoslab.pitt.edu/comir/>), CSmiRTar (<http://cosbi4.ee.ncku.edu.tw/CSmiRTar/>), and mirDIP 4.1 (<http://ophid.utoronto.ca/mirDIP/>; refs. 69–71). KEGG and GO analyses were used to define the biological pathways and the functional roles of miRNA-300 and *TUG1* targets were performed using miR-Path v.3 (snf-515788.vm.oceanos.grnet.gr). *MIR300* and *TUG1* individual gene expression profiles were obtained from curated datasets in the Gene Expression Omnibus (GEO) repository (ncbi.nlm.nih.gov/geoprofiles/). *TUG1* levels in normal and leukemic myelopoiesis were analyzed from BloodSpot database (servers.binf.ku.dk/bloodspot/) of healthy and malignant hematopoiesis. Integration of StarBase v2.0 (starbase.sysu.edu.cn/starbase2/index.php) database with the RNAseq MiRbase data from CD34⁺CD38⁻, CD34⁺CD38⁺ CML and NBM cells was used to identify *TUG1*-sponged miRNAs.

Statistical Analysis

P values were calculated by Student *t* test (GraphPad Prism v6.0). Results are shown as mean ± SEM. A *P* value less than 0.05 was considered significant (*, *P* < 0.05; **, *P* < 0.01; ***, *P* < 0.001; ****, *P* < 0.0001). Mixed models' approach, the split-plot design, was used to assess differences in percent cell across three treatment groups. The percent cell change was estimated using a model with two main effects for treatment and stage of a cell cycle, as well as their interaction. Tests of fixed effects revealed that interaction of treatment and stage of a cell cycle is highly significant (*P* = 0.01) and the two main effects, treatment and stage, should be interpreted with caution (*P* values are 1.0 and <0.0001, respectively). The differences in average percent cell were tested across groups and sliced at a particular stage of cell cycle.

Disclosure of Potential Conflicts of Interest

D. Perrotti has ownership interest in patents 8,633,161; 9,220,706 and 8,318,812. P. Neviani has ownership interest in patents 9,220,706; 8,633,161. C.J. Walker is a consultant at Karyopharm Therapeutics, Inc. F. Stagno has received speakers bureau honoraria from Novartis, Bristol-Myers Squibb, Pfizer, and Incyte. P. Vigneri reports receiving a commercial research grant from Novartis, has received speakers bureau honoraria from Incyte, is a consultant/advisory board member for Incyte. M.W. Deininger is a consultant/advisory board member at Blueprint, Fusion Pharma, Novartis, Sangamo, Takeda, Medscape, Incyte, Ascentage Pharma, Humana, TRM and reports receiving commercial research grants from Blueprint, Takeda, Novartis, Incyte, SPARC, Leukemia & Lymphoma Society, and Pfizer. D. Milojkovic has received speakers bureau honoraria from Novartis, Bristol-Myers Squibb, Incyte, and Pfizer. No potential conflicts of interest were disclosed by the other authors.

Authors' Contributions

G. Silvestri: investigation, methodology. **R. Trotta:** supervision, funding acquisition, investigation, methodology, writing-review and editing. **L. Stramucci:** investigation. **J.J. Ellis:** investigation. **J.G. Harb:** investigation. **P. Neviani:** investigation. **S. Wang:** investigation. **A. Eisfeld:** resources. **C.J. Walker:** resources. **B. Zhang:** resources. **K. Srutova:** validation, investigation. **C. Gambacorti-Passerini:** resources. **G. Pineda:** resources. **C.H.M. Jamieson:** resources. **F. Stagno:** resources. **P. Vigneri:** resources. **G. Nteliopoulos:** resources. **P.C. May:** resources. **A.G. Reid:** resources. **R. Garzon:** resources. **D. Roy:** resources. **M.M. Moutou:** investigation. **M. Guimond:** resources, investigation. **P. Hokland:** resources. **M.W. Deininger:** resources. **G. Fitzgerald:** resources. **C. Harman:** resources. **F. Dazzi:** resources. **D. Milojkovic:** resources. **J.F. Apperley:** resources. **G. Marcucci:** resources. **J. Qi:** resources. **K. Machova Polakova:** resources, investigation. **Y. Zou:** investigation. **X. Fan:** resources,

investigation. **M.R. Baer:** resources. **B. Calabretta:** resources and editing. **D. Perrotti:** conceptualization, formal analysis, supervision, funding acquisition, writing-original draft, writing-review and editing.

Acknowledgments

This work was supported by grants from the NIH-NCI CA163800 and DOD W81XWH1910166 (to D. Perrotti), ACS IRG16-123-13 Pilot Grant (to R. Trotta), Maryland Cigarette Restitution Funds (UMB Greenebaum Comprehensive Cancer Center), MSMT CZ LH15104 (to K. Machova Polakova) and CRS 16255 (to M. Guimond) for patient sample procurement and processing. S. Wang was supported by a grant from the China NSFC 81872924 and Scholarship Council (file no. 201807060002). We thank O. Goloubeva for statistical data analysis; K.F. Underwood, J.R.H. Mauban, T. Pomicter, V.H. Duong, A. Emadi, A.M. Eiring, and N.M. Glynn-Cunningham for patient sample procurement, technical assistance, reagents, and/or critical reading of the manuscript.

The costs of publication of this article were defrayed in part by the payment of page charges. This article must therefore be hereby marked *advertisement* in accordance with 18 U.S.C. Section 1734 solely to indicate this fact.

Received October 9, 2019; revised December 27, 2019; accepted February 11, 2020; published first March 4, 2020.

Abbreviations: 5-Aza-2'-deoxycytidine (5-Aza); blast crisis (BC); bone marrow (BM) microenvironment (BMM); carboxyfluorescein diacetate succinimidyl diester (CFSE); CCAAT enhancer binding protein (C/EBP); colony forming cells (CFC); chronic myelogenous leukemia (CML); chronic phase (CP); cobblestone area forming cell (CAFC); conditioned medium (CM); hematopoietic stem cell (HSC); imatinib (IM); leukemic stem cells (LSC); long term culture-initiating cells (LTC-IC); luciferase (luc); mesenchymal stromal cells (MSC); natural killer (NK); normal BM (NBM); peripheral blood (PB); PP2A activating drugs (PAD); PP2A inhibiting drugs (PID); PP2A inhibitory pathway (PIP); protein phosphatase 2A (PP2A); quiescent leukemic stem cells (qLSCs); taurine upregulated gene 1 (*TUG1*); tyrosine kinase inhibitors (TKI); umbilical cord blood (UCB).

REFERENCES

- Holyoake TL, Vetrie D. The chronic myeloid leukemia stem cell: stemming the tide of persistence. *Blood* 2017;129:1595–606.
- Radich JP, Deininger M, Abboud CN, Altman JK, Berman E, Bhatia R, et al. Chronic myeloid leukemia, version 1.2019, NCCN clinical practice guidelines in oncology. *J Natl Compr Canc Netw* 2018; 16:1108–35.
- Corbin AS, Agarwal A, Loriaux M, Cortes J, Deininger MW, Druker BJ. Human chronic myeloid leukemia stem cells are insensitive to imatinib despite inhibition of BCR-ABL activity. *J Clin Invest* 2011; 121:396–409.
- Yong AS, Keyvanfar K, Hensel N, Eniafe R, Savani BN, Berg M, et al. Primitive quiescent CD34⁺ cells in chronic myeloid leukemia are targeted by in vitro expanded natural killer cells, which are functionally enhanced by bortezomib. *Blood* 2009;113:875–82.
- Shah M, Bhatia R. Preservation of quiescent chronic myelogenous leukemia stem cells by the bone marrow microenvironment. *Adv Exp Med Biol* 2018;1100:97–110.
- Carlsten M, Jaras M. Natural killer cells in myeloid malignancies: immune surveillance, NK cell dysfunction, and pharmacological opportunities to bolster the endogenous NK cells. *Front Immunol* 2019;10:2357.

7. Ruvolo PP. The broken “Off” switch in cancer signaling: PP2A as a regulator of tumorigenesis, drug resistance, and immune surveillance. *BBA Clin* 2016;6:87–99.
8. Neviani P, Santhanam R, Trotta R, Notari M, Blaser BW, Liu S, et al. The tumor suppressor PP2A is functionally inactivated in blast crisis CML through the inhibitory activity of the BCR/ABL-regulated SET protein. *Cancer Cell* 2005;8:355–68.
9. Neviani P, Harb JG, Oaks JJ, Santhanam R, Walker CJ, Ellis JJ, et al. PP2A-activating drugs selectively eradicate TKI-resistant chronic myeloid leukemic stem cells. *J Clin Invest* 2013;123:4144–57.
10. Agarwal A, MacKenzie RJ, Pippa R, Eide CA, Oddo J, Tyner JW, et al. Antagonism of SET using OP449 enhances the efficacy of tyrosine kinase inhibitors and overcomes drug resistance in myeloid leukemia. *Clin Cancer Res* 2014;20:2092–103.
11. Perrotti D, Agarwal A, Lucas CM, Narla G, Neviani P, Odero MD, et al. Comment on “PP2A inhibition sensitizes cancer stem cells to ABL tyrosine kinase inhibitors in BCR-ABL human leukemia”. *Sci Transl Med* 2019;11:eaa0416.
12. Lai D, Chen M, Su J, Liu X, Rothe K, Hu K, et al. PP2A inhibition sensitizes cancer stem cells to ABL tyrosine kinase inhibitors in BCR-ABL(+) human leukemia. *Sci Transl Med* 2018;10:eaa8735.
13. Krause DS, Scadden DT. A hostel for the hostile: the bone marrow niche in hematologic neoplasms. *Haematologica* 2015;100:1376–87.
14. Cheloni G, Poteti M, Bono S, Masala E, Mazure NM, Rovida E, et al. The leukemic stem cell niche: adaptation to “Hypoxia” versus oncogene addiction. *Stem Cells Int* 2017;2017:4979474.
15. Saultz JN, Freud AG, Mundy-Bosse BL. MicroRNA regulation of natural killer cell development and function in leukemia. *Mol Immunol* 2019;115:12–20.
16. Ruvolo PP. The interplay between PP2A and microRNAs in leukemia. *Front Oncol* 2015;5:43.
17. Roden C, Lu J. MicroRNAs in control of stem cells in normal and malignant hematopoiesis. *Curr Stem Cell Rep* 2016;2:183–96.
18. Zhang B, Nguyen LXT, Li L, Zhao D, Kumar B, Wu H, et al. Bone marrow niche trafficking of miR-126 controls the self-renewal of leukemia stem cells in chronic myelogenous leukemia. *Nat Med* 2018;24:450–62.
19. Zhang JQ, Chen S, Gu JN, Zhu Y, Zhan Q, Cheng DF, et al. MicroRNA-300 promotes apoptosis and inhibits proliferation, migration, invasion and epithelial-mesenchymal transition via the Wnt/beta-catenin signaling pathway by targeting CUL4B in pancreatic cancer cells. *J Cell Biochem* 2018;119:1027–40.
20. Walker CJ, Oaks JJ, Santhanam R, Neviani P, Harb JG, Ferenchak G, et al. Preclinical and clinical efficacy of XPO1/CRM1 inhibition by the karyopherin inhibitor KPT-330 in Ph+ leukemias. *Blood* 2013;122:3034–44.
21. Jena N, Deng M, Sicinska E, Sicinski P, Daley GQ. Critical role for cyclin D2 in BCR/ABL-induced proliferation of hematopoietic cells. *Cancer Res* 2002;62:535–41.
22. Laurenti E, Frelin C, Xie S, Ferrari R, Dunant CF, Zandi S, et al. CDK6 levels regulate quiescence exit in human hematopoietic stem cells. *Cell Stem Cell* 2015;16:302–13.
23. Moradi S, Sharifi-Zarchi A, Ahmadi A, Mollamohammadi S, Stubenvoll A, Gunther S, et al. Small RNA sequencing reveals Dlk1-Dio3 locus-embedded MicroRNAs as major drivers of ground-state pluripotency. *Stem Cell Reports* 2017;9:2081–96.
24. Desplat V, Faucher JL, Mahon FX, Dello Sbarba P, Praloran V, Ivanovic Z. Hypoxia modifies proliferation and differentiation of CD34(+) CML cells. *Stem Cells* 2002;20:347–54.
25. Guerzoni C, Bardini M, Mariani SA, Ferrari-Amorotti G, Neviani P, Panno ML, et al. Inducible activation of CEBPB, a gene negatively regulated by BCR/ABL, inhibits proliferation and promotes differentiation of BCR/ABL-expressing cells. *Blood* 2006;107:4080–9.
26. Hayashi Y, Hirai H, Kamio N, Yao H, Yoshioka S, Miura Y, et al. C/EBPbeta promotes BCR-ABL-mediated myeloid expansion and leukemia stem cell exhaustion. *Leukemia* 2013;27:619–28.
27. Pierson BA, Miller JS. CD56+bright and CD56+dim natural killer cells in patients with chronic myelogenous leukemia progressively decrease in number, respond less to stimuli that recruit clonogenic natural killer cells, and exhibit decreased proliferation on a per cell basis. *Blood* 1996;88:2279–87.
28. Ilander M, Olsson-Stromberg U, Schlums H, Guilhot J, Bruck O, Lahteenmaki H, et al. Increased proportion of mature NK cells is associated with successful imatinib discontinuation in chronic myeloid leukemia. *Leukemia* 2017;31:1108–16.
29. Siegel G, Schafer R, Dazzi F. The immunosuppressive properties of mesenchymal stem cells. *Transplantation* 2009;87(9 Suppl):S45–9.
30. Trotta R, Ciarlariello D, Dal Col J, Mao H, Chen L, Briercheck E, et al. The PP2A inhibitor SET regulates granzyme B expression in human natural killer cells. *Blood* 2011;117:2378–84.
31. Hughes A, Yong ASM. Immune effector recovery in chronic myeloid leukemia and treatment-free remission. *Front Immunol* 2017;8:469.
32. Holyoake T, Jiang X, Eaves C, Eaves A. Isolation of a highly quiescent subpopulation of primitive leukemic cells in chronic myeloid leukemia. *Blood* 1999;94:2056–64.
33. Ma F, Wang SH, Cai Q, Jin LY, Zhou D, Ding J, et al. Long non-coding RNA TUG1 promotes cell proliferation and metastasis by negatively regulating miR-300 in gallbladder carcinoma. *Biomed Pharmacother* 2017;88:863–9.
34. Ghaforui-Fard S, Vafaei R, Taheri M. Taurine-upregulated gene 1: a functional long noncoding RNA in tumorigenesis. *J Cell Physiol* 2019;234:17100–12.
35. Qin CF, Zhao FL. Long non-coding RNA TUG1 can promote proliferation and migration of pancreatic cancer via EMT pathway. *Eur Rev Med Pharmacol Sci* 2017;21:2377–84.
36. Blank U, Karlsson S. TGF-beta signaling in the control of hematopoietic stem cells. *Blood* 2015;125:3542–50.
37. Hou Y, Li W, Sheng Y, Li L, Huang Y, Zhang Z, et al. The transcription factor Foxm1 is essential for the quiescence and maintenance of hematopoietic stem cells. *Nat Immunol* 2015;16:810–8.
38. Li Y, Zhang T, Zhang Y, Zhao X, Wang W. Targeting the FOXM1-regulated long noncoding RNA TUG1 in osteosarcoma. *Cancer Sci* 2018;109:3093–104.
39. Mancini M, Castagnetti F, Soverini S, Leo E, De Benedittis C, Gugliotta G, et al. FOXM1 transcription factor: a new component of chronic myeloid leukemia stem cell proliferation advantage. *J Cell Biochem* 2017;118:3968–75.
40. Abraham SA, Hopcroft LE, Carrick E, Drotar ME, Dunn K, Williamson AJ, et al. Dual targeting of p53 and c-MYC selectively eliminates leukaemic stem cells. *Nature* 2016;534:341–6.
41. Copland M, Hamilton A, Elrick LJ, Baird JW, Allan EK, Jordanides N, et al. Dasatinib (BMS-354825) targets an earlier progenitor population than imatinib in primary CML but does not eliminate the quiescent fraction. *Blood* 2006;107:4532–9.
42. Ciccone M, Calin GA, Perrotti D. From the biology of PP2A to the PADs for therapy of hematologic malignancies. *Front Oncol* 2015;5:21.
43. Shu J, Xia Z, Li L, Liang ET, Slipek N, Shen D, et al. Dose-dependent differential mRNA target selection and regulation by let-7a-7f and miR-17-92 cluster microRNAs. *RNA Biol* 2012;9:1275–87.
44. Eiring AM, Neviani P, Santhanam R, Oaks JJ, Chang JS, Notari M, et al. Identification of novel posttranscriptional targets of the BCR/ABL oncoprotein by ribonomics: requirement of E2F3 for BCR/ABL leukemogenesis. *Blood* 2008;111:816–28.
45. Konishi H, Fujiya M, Ueno N, Moriuchi K, Sasajima J, Ikuta K, et al. microRNA-26a and -584 inhibit the colorectal cancer progression through inhibition of the binding of hnRNP A1-CDK6 mRNA. *Biochem Biophys Res Commun* 2015;467:847–52.
46. Perrotti D, Neviani P. Protein phosphatase 2A: a target for anticancer therapy. *Lancet Oncol* 2013;14:e229–38.
47. Du C, Pan P, Jiang Y, Zhang Q, Bao J, Liu C. Microarray data analysis to identify crucial genes regulated by CEBPB in human SNB19 glioma cells. *World J Surg Oncol* 2016;14:258.
48. Luedde T, Duderstadt M, Streetz KL, Tacke F, Kubicka S, Manns MP, et al. C/EBP beta isoforms LIP and LAP modulate progression of the cell cycle in the regenerating mouse liver. *Hepatology* 2004;40:356–65.
49. Zিপeto MA, Court AC, Sadarangani A, Delos Santos NP, Balaian L, Chun HJ, et al. ADAR1 activation drives leukemia stem cell self-renewal by impairing let-7 biogenesis. *Cell Stem Cell* 2016;19:177–91.

50. Pellicano F, Park L, Hopcroft LEM, Shah MM, Jackson L, Scott MT, et al. hsa-mir183/EGR1-mediated regulation of E2F1 is required for CML stem/progenitor cell survival. *Blood* 2018;131:1532–44.
51. Kijima M, Gardiol N, Held W. Natural killer cell mediated missing-self recognition can protect mice from primary chronic myeloid leukemia in vivo. *PLoS One* 2011;6:e27639.
52. Baginska J, Viry E, Paggetti J, Medves S, Berchem G, Moussay E, et al. The critical role of the tumor microenvironment in shaping natural killer cell-mediated anti-tumor immunity. *Front Immunol* 2013;4:490.
53. Hasmim M, Messai Y, Ziani L, Thiery J, Bouhris JH, Noman MZ, et al. Critical role of tumor microenvironment in shaping NK cell functions: implication of hypoxic stress. *Front Immunol* 2015;6:482.
54. Schepers K, Campbell TB, Passegue E. Normal and leukemic stem cell niches: insights and therapeutic opportunities. *Cell Stem Cell* 2015;16:254–67.
55. Trotta R, Chen L, Costinean S, Josyula S, Mundy-Bosse BL, Ciarlariello D, et al. Overexpression of miR-155 causes expansion, arrest in terminal differentiation and functional activation of mouse natural killer cells. *Blood* 2013;121:3126–34.
56. Costinean S, Sandhu SK, Pedersen IM, Tili E, Trotta R, Perrotti D, et al. Src homology 2 domain-containing inositol-5-phosphatase and CCAAT enhancer-binding protein beta are targeted by miR-155 in B cells of E-micro-MiR-155 transgenic mice. *Blood* 2009;114:1374–82.
57. Zhao L, Sun H, Kong H, Chen Z, Chen B, Zhou M. The Lncrna-TUG1/EZH2 axis promotes pancreatic cancer cell proliferation, migration and EMT phenotype formation through sponging Mir-382. *Cell Physiol Biochem* 2017;42:2145–58.
58. Katsushima K, Natsume A, Ohka F, Shinjo K, Hatanaka A, Ichimura N, et al. Targeting the Notch-regulated non-coding RNA TUG1 for glioma treatment. *Nat Commun* 2016;7:13616.
59. Traer E, MacKenzie R, Snead J, Agarwal A, Eiring AM, O'Hare T, et al. Blockade of JAK2-mediated extrinsic survival signals restores sensitivity of CML cells to ABL inhibitors. *Leukemia* 2012;26:1140–3.
60. Klingemann H, Boissel L, Toneguzzo F. Natural killer cells for immunotherapy - advantages of the NK-92 cell line over blood NK cells. *Front Immunol* 2016;7:91.
61. Schepers K, Pietras EM, Reynaud D, Flach J, Binnewies M, Garg T, et al. Myeloproliferative neoplasia remodels the endosteal bone marrow niche into a self-reinforcing leukemic niche. *Cell Stem Cell* 2013;13:285–99.
62. Oaks JJ, Santhanam R, Walker CJ, Roof S, Harb JG, Ferenchak G, et al. Antagonistic activities of the immunomodulator and PP2A-activating drug FTY720 (Fingolimod, Gilenya) in Jak2-driven hematologic malignancies. *Blood* 2013;122:1923–34.
63. Eiring AM, Harb JG, Neviani P, Garton C, Oaks JJ, Spizzo R, et al. miR-328 functions as an RNA decoy to modulate hnRNP E2 regulation of mRNA translation in leukemic blasts. *Cell* 2010;140:652–65.
64. Pineda G, Lennon KM, Delos Santos NP, Lambert-Fliszar F, Riso GL, Lazzari E, et al. Tracking of normal and malignant progenitor cell cycle transit in a defined niche. *Sci Rep* 2016;6:23885.
65. Roccaro AM, Sacco A, Maiso P, Azab AK, Tai YT, Reagan M, et al. BM mesenchymal stromal cell-derived exosomes facilitate multiple myeloma progression. *J Clin Invest* 2013;123:1542–55.
66. Thery C, Amigorena S, Raposo G, Clayton A. Isolation and characterization of exosomes from cell culture supernatants and biological fluids. *Curr Protoc Cell Biol* 2006;Chapter 3:Unit 3 22.
67. Neviani P, Santhanam R, Oaks JJ, Eiring AM, Notari M, Blaser BW, et al. FTY720, a new alternative for treating blast crisis chronic myelogenous leukemia and Philadelphia chromosome-positive acute lymphocytic leukemia. *J Clin Invest* 2007;117:2408–21.
68. Romee R, Rosario M, Berrien-Elliott MM, Wagner JA, Jewell BA, Schappe T, et al. Cytokine-induced memory-like natural killer cells exhibit enhanced responses against myeloid leukemia. *Sci Transl Med* 2016;8:357ra123.
69. Coronello C, Benos PV. ComiR: combinatorial microRNA target prediction tool. *Nucleic Acids Res* 2013;41:W159–64.
70. Tokar T, Pastrello C, Rossos AEM, Abovsky M, Hauschild AC, Tsay M, et al. mirDIP 4.1-integrative database of human microRNA target predictions. *Nucleic Acids Res* 2018;46:D360–70.
71. Wu WS, Tu BW, Chen TT, Hou SW, Tseng JT. CSmiRTar: condition-specific microRNA targets database. *PLoS One* 2017;12:e0181231.

SUPPEMENTARY FIGURES

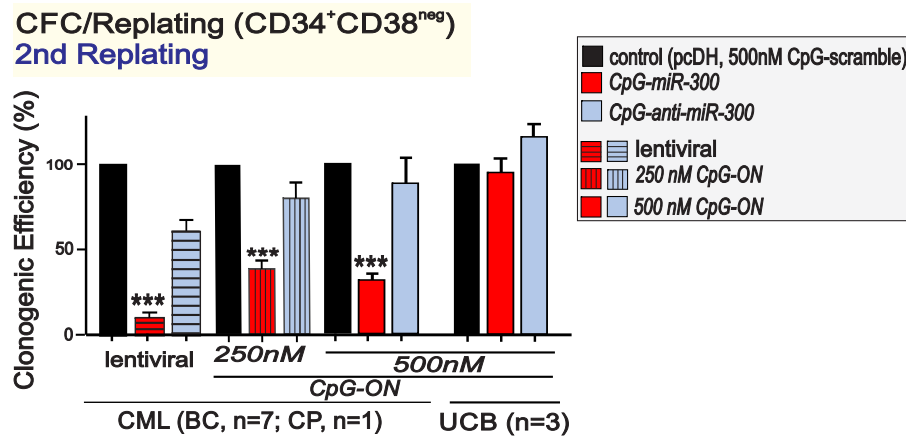


Figure S1. *MIR300* activity in quiescent leukemic stem and progenitor cells. CFC-replating assays shows effects of lentiviral-mediated ectopic *MIR300* expression, 250 nM and 500 nM *CpG-miR-300* on serial replating activity (2nd replating) of leukemic chronic and acute CML and normal UCB CD34⁺CD38⁻HSC-enriched cell fractions. Infection with lentiviral empty vector and treatment with CpG-anti-*MIR300* and CpG-scramble served as controls.

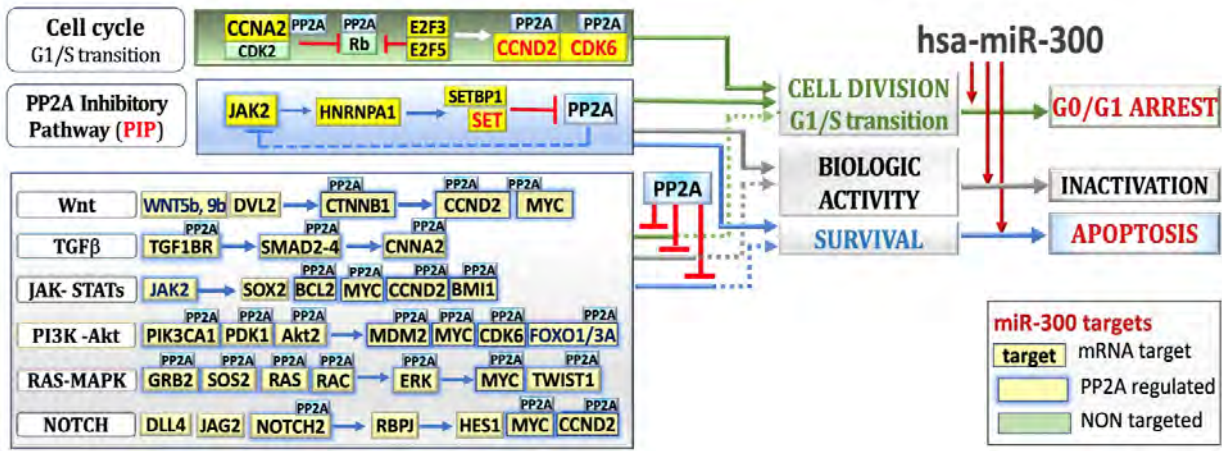


Figure S2. KEGG/GO analysis of *MIR300* on PP2A-regulated signal transduction pathways. Cartoon shows the SET-dependent PP2A Inhibitory pathway in CML and the pleiotropic inhibitory effect of PP2A activation on validated and predicted *MIR300* targets regulating G1/S cell cycle transition, Wnt- β -catenin, TGF β , JAK-STAT, PI-3K-Akt, RAS-MAPK and Notch signaling pathways.

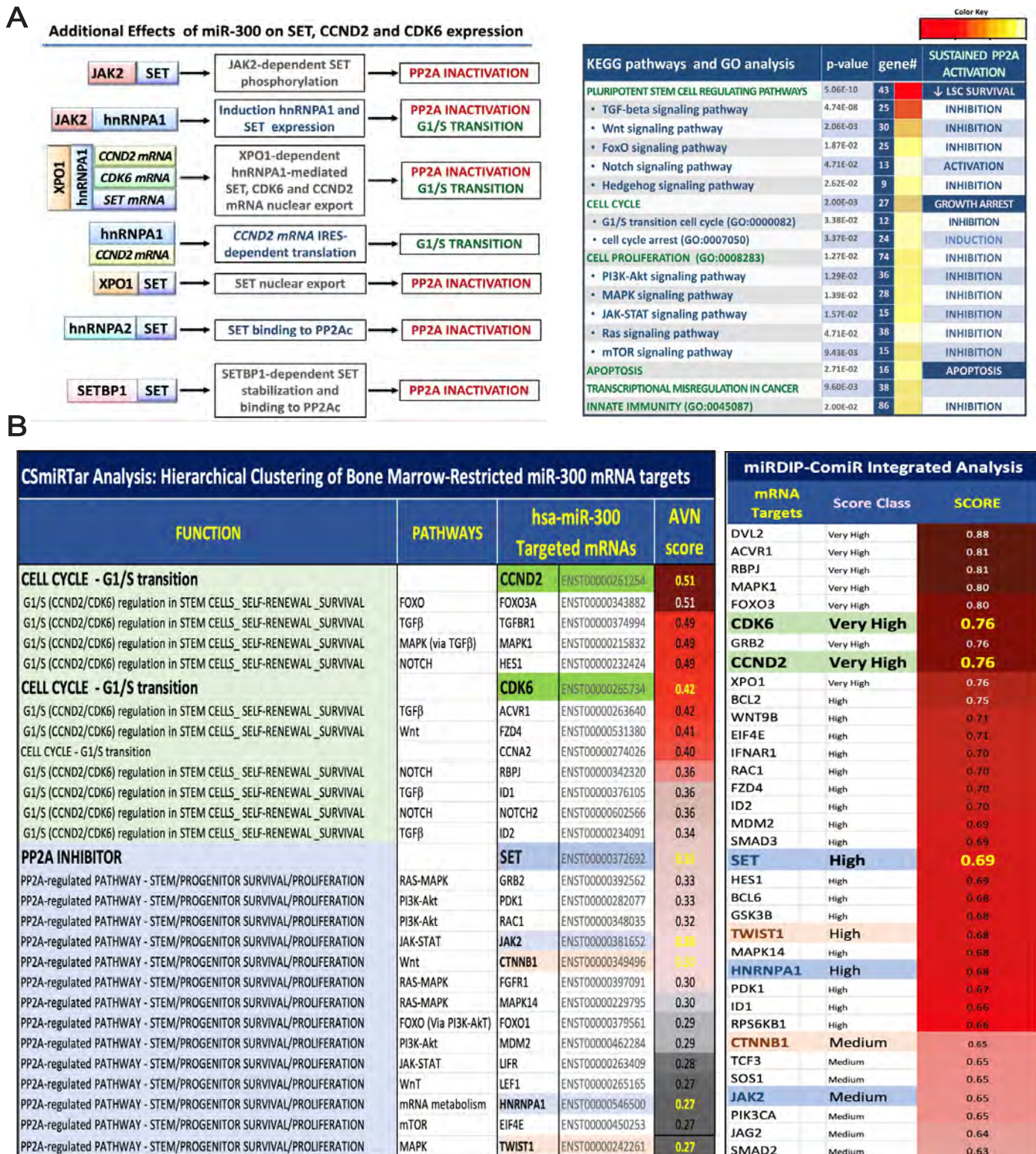


Figure S3. MIR300 acts as master PP2A activator and inhibitor of G1/S transition. A, (left) Additional effects of MIR300 on SET, CCND2 and CDK6 expression; (right) KEGG/GO analysis of MIR300 effects on signal transduction pathways. B, CSmiRTar (filters: bone marrow normal and myeloid leukemia cells) and miRDIP-ComiR integrated analyses show functional clustering of predicted/validated MIR300 targets.

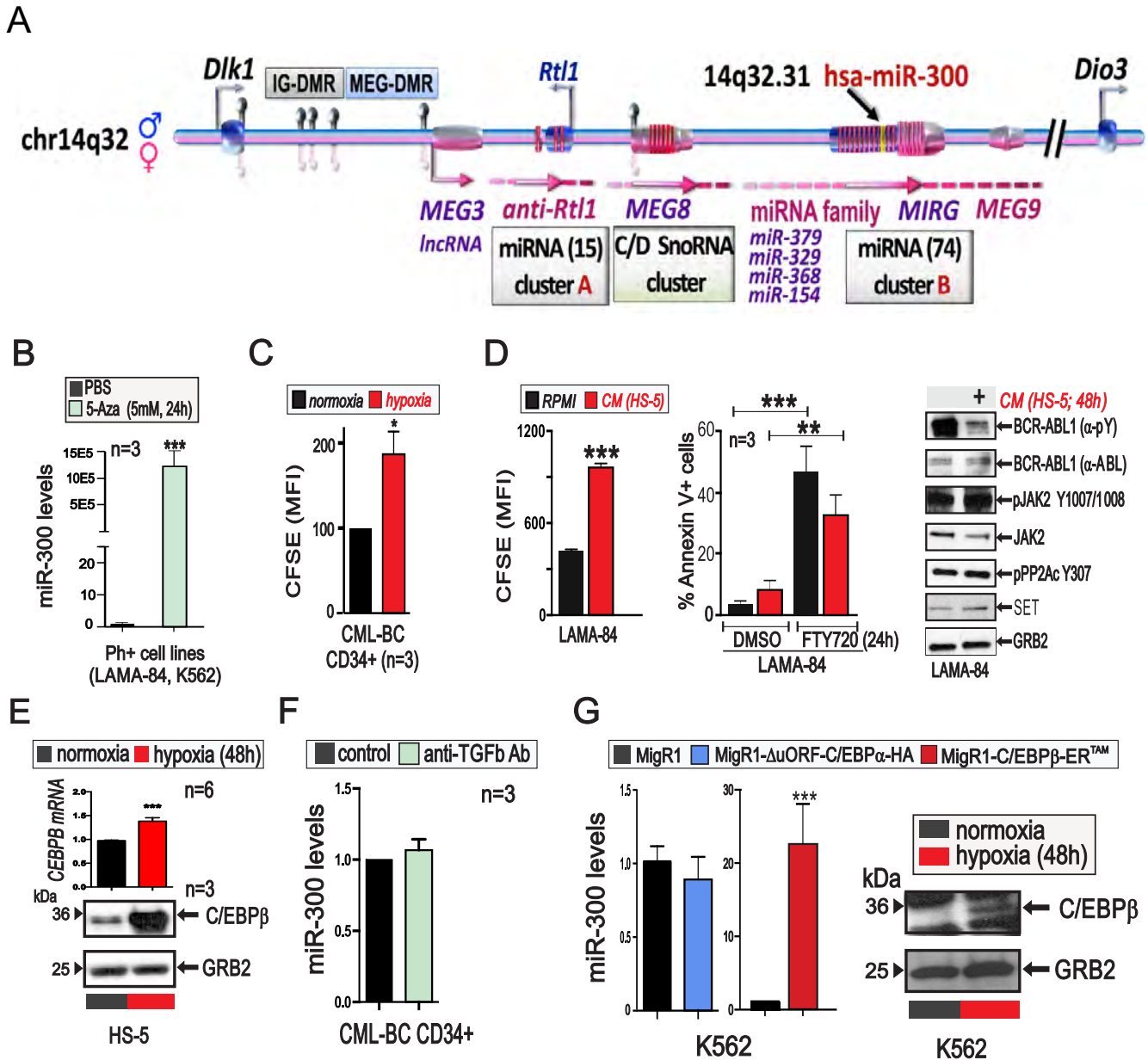


Figure S4. *MIR300* anti-proliferative activity accounts for BMM-induced LSC entry into quiescence.

A, Structure of 14q32 *DLK1-DIO3* genomic imprinted locus hosting the MEG3-regulated human *MIR300*. **B**, *MIR300* levels in 5-Aza- or DMSO-treated (24h) Ph⁺ cells. **C**, Effect of hypoxia on proliferation of CFSE⁺CD34⁺ CML-BC cells. **D**, left: Effect of MSC (HS-5)-derived CM on LAMA-84 proliferation expressed as fold changes of CFSE mean of fluorescence intensity (MFI)±SEM; middle: pro-apoptotic effect of PAD (FTY720; 2.5μM) and DMSO (control) on HS-5-cultured LAMA-84 cells; right: Effect of MSC (HS-5)-derived CM BCR-ABL1 expression (α-ABL1) and activity (α-PY), phospho-BCR-ABL1, JAK2 expression and activity JAK2 Y1007/1008, PP2A activity (pPPP2AY307 inactive form) and GRB2 used as a control (blots are representative of three independent experiments). **E**, Levels of C/EBPβ and GRB2 mRNA and protein in HS-5 cells exposed to hypoxia (48h; 1% O₂). **F**, Effect of neutralizing TGFβ antibody (anti-TGFβ Ab; 48h, 1.25 μg/ml) on *MIR300* levels in CD34⁺ CML-BC cells. **G**, Effect of ectopic C/EBPα (MigR1-ΔuORF-C/EBPα-HA) and C/EBPβ (MigR1-C/EBPβ-ER^{TAM}) on *MIR300* levels in K562 cells. Immunoblot shows levels of C/EBPβ and GRB2 in normoxic and hypoxic K562 cells.

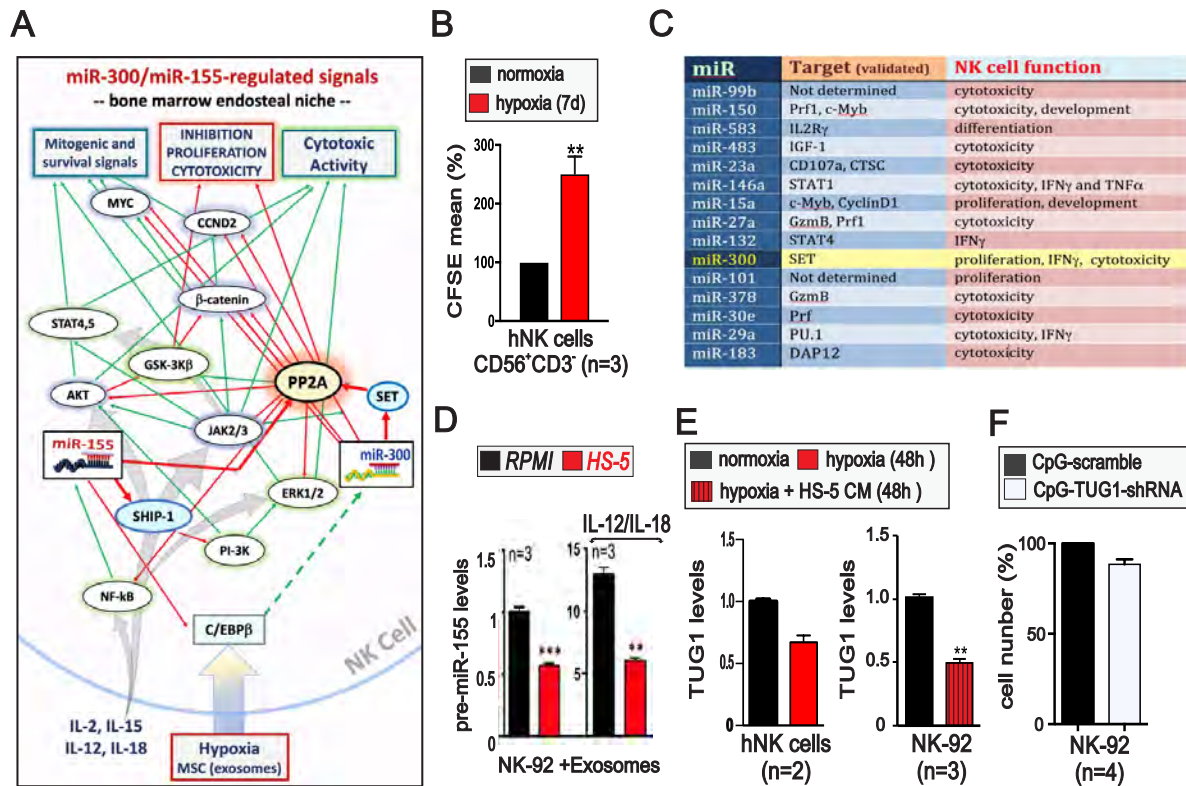


Figure S5. BMM-induced *MIR300* anti-proliferative and PP2A-activating functions impair NK cell immune-response. **A**, PP2A-dependent regulation of *MIR300* and miR-155 validated pathways predicted to occur also in the bone marrow endosteal niche. **B**, Effect of hypoxia (1% O₂, 7 days) on CFSE⁺NK cell proliferation (% CFSE mean of fluorescence). **C**, HS-5 exosomal miRNAs reported as negative regulators of NK cell proliferation/activity and their experimentally validated targets. miRNA RNAseq was performed on an Illumina platform using libraries derived from 100 ng RNA/sample from HS-5 exosome purifications (n=3). **D**, Precursor (*pre-miR-155*) miR-155 (BIC) levels in resting and IL-12/IL-18 (18h)-stimulated NK cells exposed (48h) to HS-5 exosomes. **E**, Effect of hypoxia (1% O₂) and HS-5 CM (48h) on TUG1 expression in CD56⁺CD3⁺ primary NK and NK-92 cells. **F**, Effect of *CpG-TUG1-shRNA* and *CpG-scramble* (200-500 nM, 5 days) on IL-2-induced NK cell proliferation (% cell number). Data are represented as mean \pm SEM.

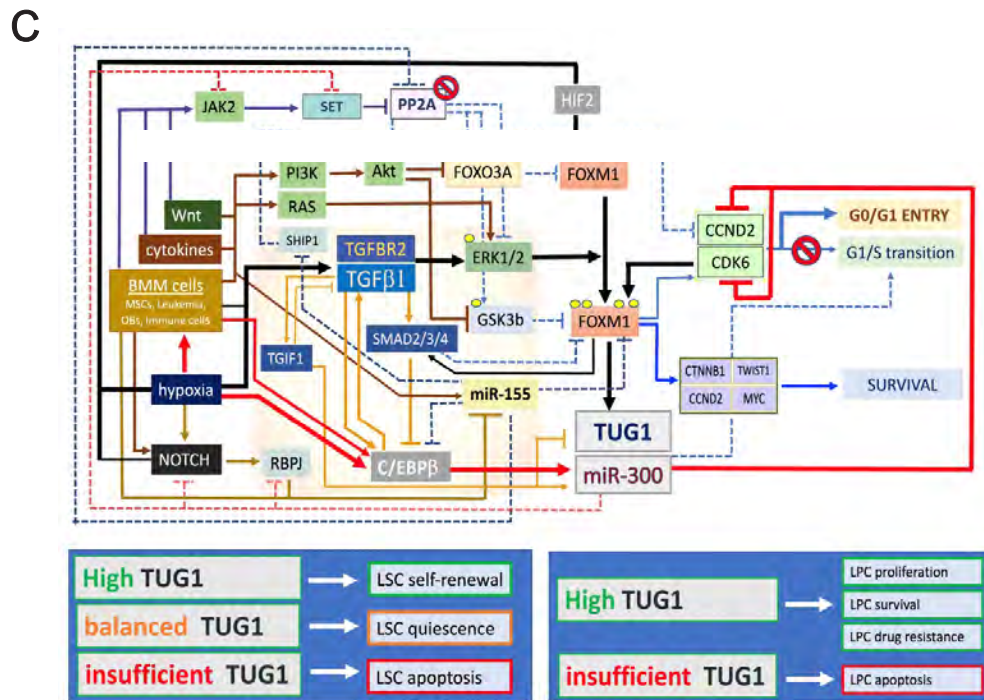
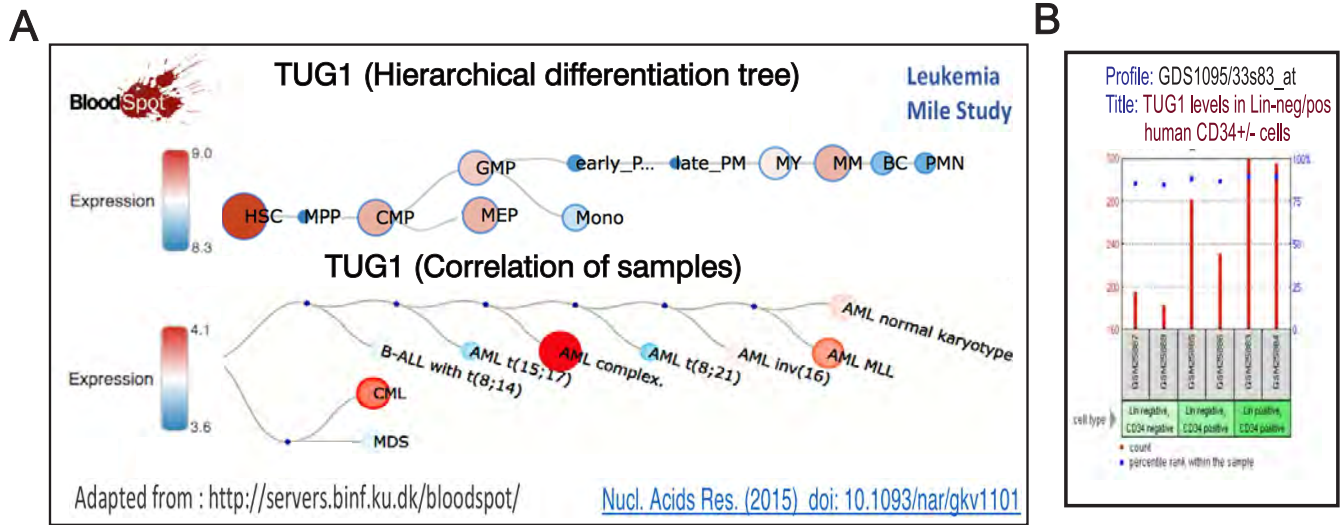


Figure S6. Selective suppression of *MIR300* pro-apoptotic but not anti-proliferative activity by TUG1 lncRNA in quiescent LSCs. **A**, BloodSpot array-based TUG1 expression levels during normal myelopoiesis and in myeloid neoplasms. **B**, GEO Profiles show TUG1 levels in lineage-negative (Lin⁻) and -positive (Lin⁺) CD34⁻ and CD34⁺ human stem/progenitor cells from healthy individuals. **C**, Experimental data- and current literature-based graphic representation of signaling network controlling CML LSC quiescence and survival through the BMM-C/EBP β -*MIR300* and BMM-TGF β -FoxM1 pathways. Dotted lines indicate inactive pathways, line thickness indicates relevance of the signal for LSC quiescence. Red lines indicate signals increasing *MIR300* levels. Black lines signals increasing TUG1 levels. (*bottom*) effects of different TUG1 levels on CML leukemic stem (LSC) and progenitor (LPC) cell fate.

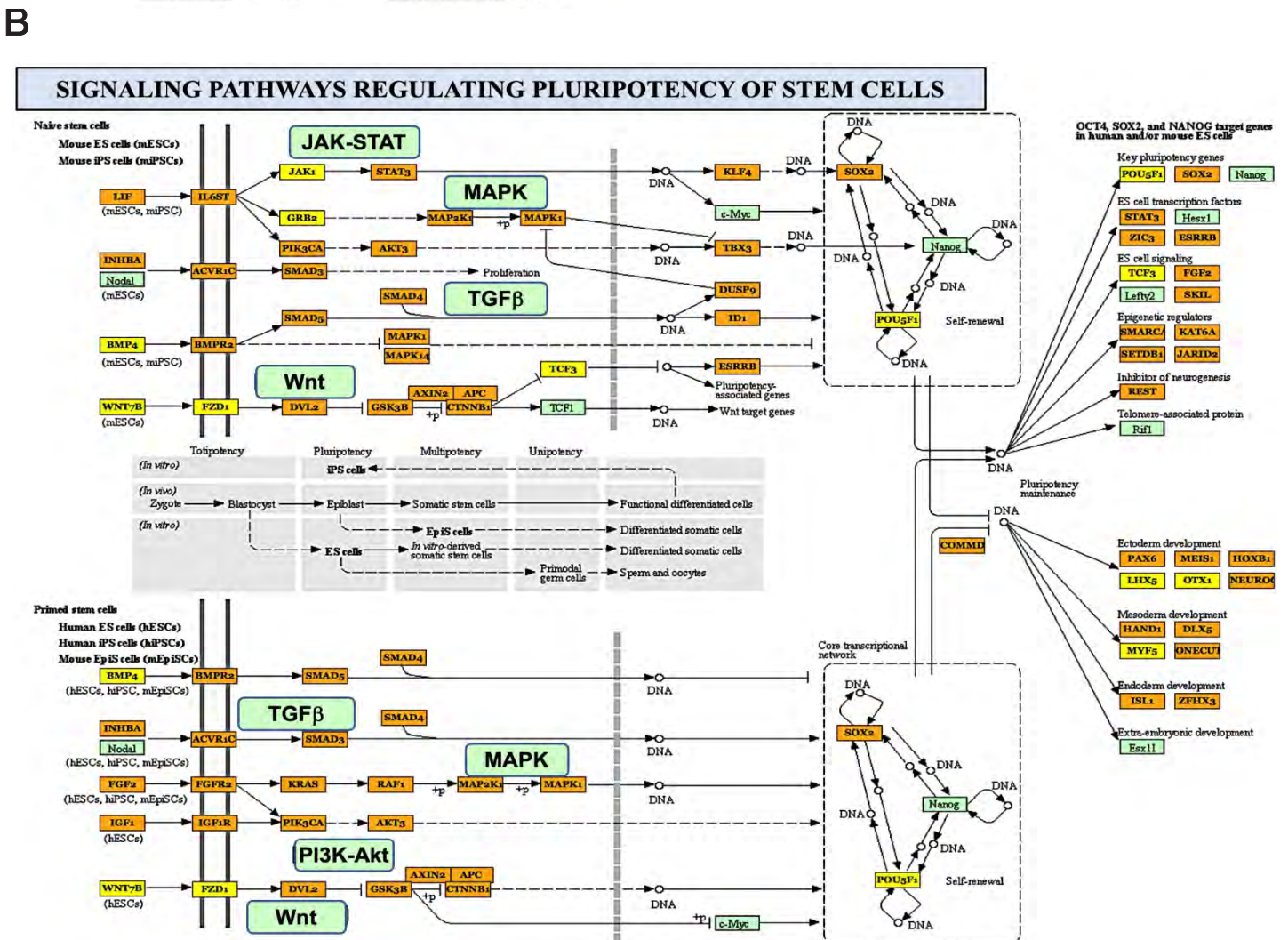
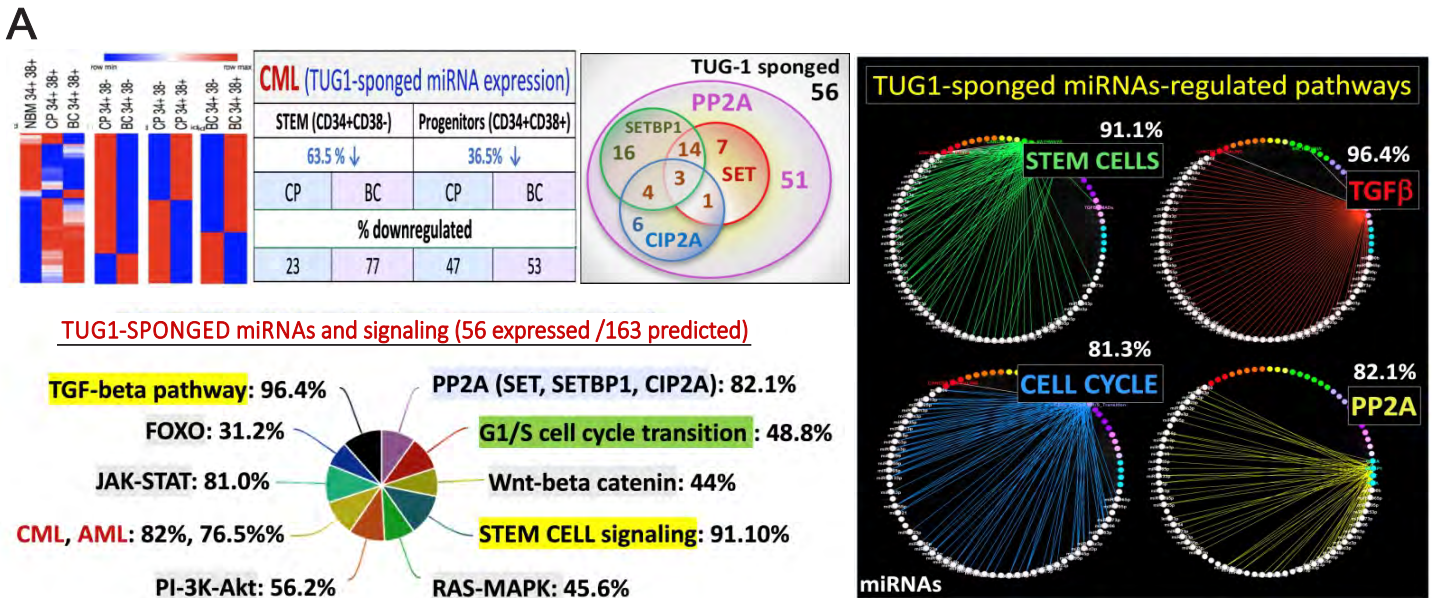


Figure S7. Bioinformatic analysis of TUG1-sponged miRNAs and mRNA targets in CML. A, (left) Integration of validated TUG1-sponged miRNAs with RNAseq data (heatmaps) from BM CD34+CD38- and CD34+CD38+ CML (CP and BC) and NBM (n=3/group). Effect of TUG1-sponged miRNA on PP2A inhibitors (Venn diagram); Functional integration of TUG1-sponged miRNAs and their mRNA targets into regulatory network KEGG/GO analysis; (right) Circular diagrams show top 4 pathways affected by TUG1-sponged miRNAs. B, Predicted effect of MIR300 and of TUG1-sponged miRNAs on Pluripotent Stem Cell Signaling pathways.

Figures	Range values of controls for the indicated experiments
Figure 2A	<u>Cell Viability</u> SCR 130000 to 250000 cell/ml <u>CFCs</u> SCR UCB 193 to 220 colonies/number of plated cells SCR CML BC 182 to 200 colonies/ number of plated cells
Figure 2D	<u>CFSE tracking cell number</u> CpG SCR Oligos 250 nM 313 to 499 CD34 ⁺ qLSCs CpG SCR Oligos 250 nM 1874 to 9864 Div. 1-2 CD34 ⁺ CML progenitors CpG SCR Oligos 500 nM 104 to 2477 CD34 ⁺ qLSCs CpG SCR Oligos 500 nM 722 to 88464 Div. 1-2 CD34 ⁺ CML progenitors <u>LTC-IC assays</u> Lentiviral pcDH infection: 98 to 180 colonies CML CpG SCR Oligos 500 nM: 80 to 146 colonies CML CpG SCR Oligos 250 nM: 81 to 210 colonies UCB CpG SCR Oligos 500 nM: 148 to 194 colonies
Figure 4C	<u>Growth inhibition %</u> Control RPMI leukemia cells/ml: 0.14 to 1.34 10 ³ /ml
Figure 4D	<u>Real Time PCR</u> Normoxia-cultured cells: 30.4 to 32.6 CT
Figure 4F	<u>Real Time PCR</u> MigRI-transduced cells: 27.5 to 32.9 CT
Figure 5A	<u>CFSE-mediated proliferation:</u> Control 318 to 677 CD34 ⁺ qLSCs
Figure 5D	<u>Growth inhibition %</u> Control RPMI or SCR NK cells/ml: 0.46 to 1.35x10 ³
Figure 5F	<u>Cell number %</u> SCR NK cells/ml: 0.468 to 2.31x10 ³
Figure 6E	<u>CFSE tracking cell number</u> SCR 116 to 953 CD34 ⁺ qLSCs SCR 15076 to 61621 Div. 1-2 CD34 ⁺ progenitors
Figure 7C	<u>FACS analysis</u> CpG SCR hCD45 ⁺ CD34 ⁺ in mouse BM 44.79% to 80% CpG SCR hCD45 ⁺ CD34 ⁺ CD38 ⁻ in mouse BM 0.4% to 1.88% CpG SCR hCD45 ⁺ CD34 ⁺ CD38 ⁻ CD90 ⁺ in mouse BM 0.00044% to 0.008%
Figure 7E	<u>FACS analysis</u> CpG SCR hCD45 ⁺ in mouse BM 43.5% to 87.3% CpG SCR hCD45 ⁺ in mouse PB 0% to 87%

Table S1. Range values of controls for the experiment reported in the indicated figures (see Methods for further details).